Flow Measuring Techniques in Steady and Pulsating Compressible Flows

by

Fredrik Laurantzon

Fredrik Laurantzon 2010, **Flow Measuring Techniques in Steady and Pulsating Compressible Flows**

KTH Mechanics, SE-100 44 Stockholm, Sweden

Abstract

This thesis deals with flow measuring techniques applied on steady and pulsating flows. Specifically, it is focused on gas flows where density changes can be significant, i.e. compressible flows. In such flows only the mass flow rate has a significance and not the volume flow rate since the latter depends on the pressure. The motivation for the present study is found in the use of flow meters for various purposes in the gas exchange system for internal combustion engines. Applications can be found for instance regarding measurements of air flow to the engine, or measurements of the amount of exhaust gas recirculation. However the scope of thesis is wider than this, since the thesis aims to investigate the response of flow meters to pulsating flows. The study is mainly experimental, but it also includes an introduction and discussion of several in industry, common flow measuring techniques.

The flow meters were studied using a newly developed flow rig, designed for measurement of steady and pulsating air flow of mass flow rates and pulse frequencies typically found in the gas exchange system of cars and smaller trucks. Flow rates are up to about 200 g/s and pulsation frequencies from 0 Hz (i.e. steady flow) up to 80 Hz. The study included the following flow meters: hot-film mass flow meter, venturi flowmeter, Pitot tube, vortex flowmeter and turbine flowmeter. The performance of these meters were evaluated at both steady and pulsating conditions. Furthermore, the flow under both steady and pulsating conditions were characterized by means of a resistance-wire based mass flow meter, with the ability to perform time resolved measurements of both the mass flux ρu, and the stagnation temperature T_0.

Experiments shows that, for certain flow meters, a quasi-steady assumption is fairly well justified at pulsating flow conditions. This means that the fundamental equations describing the steady flow, for each instant of time, is applicable also in the pulsating flow. In the set-up, back-flow occurred at certain pulse frequencies, which can result in highly inaccurate output from certain flow meters, depending on the measurement principle. For the purpose of finding means to determine when back flow prevails, LDV measurements were also carried out. These measurements were compared with measurements using a vortex flow meter together with a new signal processing technique based on wavelet analysis. The comparison showed that this technique may have a potential to measure pulsating flow rates accurately.

Descriptors: Flow measuring, compressible flow, steady flow, pulsating flow, hot-wire anemometry, cold-wire anemometry.

Preface

This licentiate thesis in fluid mechanics deals with flow measurement techniques applied on steady and pulsating compressible flows. It is mainly based on experimental work. The thesis is divided into two parts, where Part I comprises a review of flow measuring techniques and a summary of the results, whereas Part II consists of four papers. With the exception of Paper 4, the papers in Part II are unaltered from their respective original format, since they all have been published. Paper 4 is in its present form a technical note but will complemented and thereafter submitted. In Chap. 8 of Part I in the thesis, the respondent's contributions to all papers are stated.

November 2010, Stockholm

Fredrik Laurantzon

However beautiful the strategy, you should occasionally look at the results.

Sir Winston Churchill (1874–1965)

Contents

Part I

Overview and summary

CHAPTER 1

Introduction

This thesis deals with flow metering for both stationary and pulsating flows. Specifically, it is focused on measurements of gas flows where density changes can be significant, i.e. compressible flows. The study is mainly experimental, but includes also an introduction to several in industry, common flow measuring techniques. It is motivated by the need to accurately measure mass flow rates of gas/air flows in internal combustion engines, both directly on the engine during normal operation, but also under laboratory conditions during simulations of full engines or various engine components.

1.1. Flow metering

A flow meter is an instrument for determining the flow rate of a fluid in some sort of conduit, for instance natural gas and oil in pipelines, domestic water supply, intake air to a combustion engines etc. The necessity of accurate flow rate measurement of a fluid, is as important today as it has been in the ancient history. A typical example of one early primitive, albeit useful flow meter installation, is by the Roman engineers, who built aqueducts and piping systems, leading the water to households and public baths. The measuring device in that case, can be seen as a primitive ancestor to the *orifice plate*. However, the Romans did not fully realize what the flow rate Q depend on. It was however already known by the Egyptians some 200 years earlier, that the flow rate was dependent on the cross section area of the pipe A and the fluid velocity u, such that $Q = Au$. A more profound insight in the fundamental relationship between quantities, such as pressure, velocity and cross section area was not establish until about the 16th century. For a more exhaustive elaboration regarding the developments in flow measurement from this time on, consult e.g. Cascetta (1995).

Nowadays, the costs that are controlled by flow meters, are worldwide estimated to the order of 10 000 billion US dollars annually, as discussed in the editorial of Flow Measurement and Instrumentation (1989). Moreover *Bosch Automotive* announced recently the production of their 100 millionth hot-film mass airflow sensor (designed to measure the engine's air intake). Thus the

market for flow meters in various types of industries is quite large. It is therefore desirable for flow meters to have good performance in terms of accuracy, repeatability, and rangeability.

1.2. Steady and pulsating flow

Steady flow is a type of flow which in general can be of *turbulent* nature with random fluctuations in the flow. However, the statistical moments for the velocity u, such as mean value U and root mean square value u_{rms} are independent of time, (for long enough time series) and the autocorrelation of the signal will for long time shifts go to zero.

Pulsating flow on the other hand, is a specific type of *unsteady flow*, where a cyclic variation is superimposed on a constant (in time) flow. The statistical moments will for pulsating flow also be independent of time, but the autocorrelation will not go to zero, but show the pulsating component also for long time separations. A commonly used parameter to characterize the pulsating flow amplitude is $u_{\mathrm{rms,pulse}}/u_b$, where $u_{\mathrm{rms,pulse}}$ is the root-mean-square value of the pulsations and u_b is the *bulk-mean velocity*. For several flow meters, such as differential pressure flow meters and turbine flow meters, the metering error depends on this parameter. The parameter can in any event be quite cumbersome to determine (see Mottram 1992), since for instance in pulsating pipe flow, the pulsating and turbulence velocity fluctuations do not have to be uniform across the pipe cross-section.

The objective of the present work is to evaluate and develop flow measuring methods, that can be used in the range of typical internal combustion engine gas exchange flows. For the present work we focus on pulsating flows up to 80 Hz pulse frequency and mass flow rates up to about 200 g/s.

1.3. Thesis outline

In the following, Chap. 2 is an introduction to relevant gas dynamics concepts useful for understanding compressible flow related to flow metering, whereas Chap. 3 introduces several different flow metering devices and discusses their physical background and their application to compressible mass flow metering. In Chap. 4 the experimental set-ups, both the flow facility and the various flow meters that have been analyzed are described and in Chap. 5 the results from the experiments are shown. Chap. 6 introduces an in-house designed vortex flow meter. Finally, in Chap. 7 some concluding remarks are given. Appended to the thesis are four papers that discuss various aspects and/or methods in more detail.

Fundamental relations

In this chapter, the fundamentals of thermo- and gas-dynamics for the analysis and understanding of flow behavior in stationary and pulsating (under quasi-steady conditions), compressible flow in various flow metering situations will be discussed.

2.1. Basic thermodynamics of gases

To analyze the phenomena in compressible flows the laws of thermodynamics is a necessary ingredient. The first law of thermodynamics reads

$$de = \delta q + \delta w \tag{2.1}$$

where de is the change in internal energy when heat (δq) and/or work (δw) is added to the system. The second law of thermodynamics can be written

$$ds = \frac{\delta q}{T} + ds_{\mathrm{irrev}} \tag{2.2}$$

where s is the entropy and T the temperature. The quantity ds_{irrev} is always greater or equal to zero. Thus an alternative form of Eq. (2.2), would be

$$ds \geq \frac{\delta q}{T} \tag{2.3}$$

It should be noted here that both e and s are state variables, i.e. the change in these variables from one start condition to an end condition, does not depend on how the change was made, it only depends on the conditions at the start and end states[1].

The state law for a perfect gas can be written

$$p = \rho R T \tag{2.4}$$

where p is the pressure, ρ is the density and R the specific gas constant which for air has the value $R =$287 J/(kg K). Two other important quantities are the specific heats at constant pressure, c_p, and constant volume, c_v, which are related such that $R = c_p - c_v$ assuming that the values are constant. This is approximately true in the temperature range 5-600 K when vibrational modes of the molecules are not yet excited (a so called calorically perfect gas). The

---

[1]Here, the notation d is adopted for exact differentials, whereas δ is used for inexact differentials, i.e. for path-dependent quantities.

ratio between the specific heats are usually written as $\gamma = c_p/c_v$ and for air (or any calorically perfect gas with two-atomic molecules) $\gamma = 1.40$.

In many processes, the change of state can be seen as isentropic, i.e. the changes occur adiabatically and reversibly. It can readily be deduced from the thermodynamic laws, Eqs. (2.1), (2.2) and (2.4), that if the flow process is isentropic, i.e. $ds = 0$, then the following relation is valid

$$\frac{p}{\rho^\gamma} = \text{const.} \tag{2.5}$$

Similar relations can also be obtained between the pressure, density or temperature by using the state law Eq. (2.4) to obtain

$$\frac{p}{p_{\text{ref}}} = \left(\frac{\rho}{\rho_{\text{ref}}}\right)^\gamma = \left(\frac{T}{T_{\text{ref}}}\right)^{\gamma/(\gamma-1)} \tag{2.6}$$

where index "ref" refers to some reference condition. Note that these isentropic conditions are independent of the flow as long as it is reversible and adiabatic, i.e. there is no constraint that it should be e.g. stationary.

2.2. Gas dynamics fundamentals

2.2.1. Conservation laws

Compressible fluid flow is in principle governed by three fundamental physical conservation laws, namely, conservation of mass, momentum and energy. The perhaps most lucid description of these, is the integral formulation (see for example Anderson 2003), where we consider the conservation laws of the fluid within a fix, stationary control volume V.

Conservation of mass

$$\frac{\partial}{\partial t} \int_V \rho dV = - \int_S \rho \mathbf{u} \cdot d\mathbf{S} \tag{2.7}$$

Note from the above equation that the integrand on the right hand side is the mass flow $d\dot{m}$, through the surface $d\mathbf{S}$, where in general $d\mathbf{S}$ is an infinitesimal surface element. However, the total mass flow through a cross section A, is simply

$$\dot{m} = \rho A u \tag{2.8}$$

where u is orthogonal to the surface. Moreover from Eq. (2.8), two more quantities can be extracted, that are frequently occurring in fluid flow measurements. These are the *mass flux* and *volume flow*:

$$\dot{\mathcal{M}} = \rho u \tag{2.9}$$

$$Q = A u \tag{2.10}$$

respectively.

Conservation of momentum

$$\frac{\partial}{\partial t}\int_V \rho \mathbf{u}\,dV = -\int_S (\rho \mathbf{u}\cdot d\mathbf{S})\mathbf{u} + \int_V \rho \mathbf{f}\,dV - \int_S p\,d\mathbf{S} + \mathbf{F}_{\mathrm{visc}} \qquad (2.11)$$

The term on the left hand side corresponds to the change in momentum inside the control volume per unit time, whereas the first term on the right hand side is the net influx of momentum into the control volume. The three other terms can be viewed as source terms for momentum, corresponding to changes due to body forces on the volume, pressure forces and viscous forces ($\mathbf{F}_{\mathrm{visc}}$) acting on the surface of the control volume. Here $\mathbf{f}$ is a body force per unit mass.

Conservation of energy

$$\frac{\partial}{\partial t}\int_V \left[\rho\left(e+\frac{u^2}{2}\right)\right]dV = -\int_S \rho\left(e+\frac{u^2}{2}\right)\mathbf{u}\cdot d\mathbf{S} - \int_S p\mathbf{u}\cdot d\mathbf{S}$$
$$+ \int_V \rho(\mathbf{f}\cdot\mathbf{u})dV + \int_V \dot{q}\rho\,dV \qquad (2.12)$$

In the energy equation the left hand side expresses the changes of energy per unit time of the fluid inside the control volume where the energy is the sum of the inner (microscopic) energy (e) and the macroscopic kinetic energy ($\frac{1}{2}u^2$). The terms of the right hand side are respectively, net transport of energy into the control volume, work carried out by pressure forces, work carried out by body forces and finally heat transferred to the volume.

2.2.2. One-dimensional flow

By assuming that the flow is stationary and one-dimensional, i.e. the flow is in one direction inside a *stream tube*, there are no variations over the cross section and the cross section area (A) of the control volume is constant, the three conservation laws become

$$\rho_1 u_1 = \rho_2 u_2 \qquad (2.13)$$

$$p_1 + \rho_1 u_1^2 = p_2 + \rho_2 u_2^2 \qquad (2.14)$$

$$h_1 + \frac{1}{2}u_1^2 = h_2 + \frac{1}{2}u_2^2 + \dot{q} \qquad (2.15)$$

where the enthalpy $h = c_p T$ has been introduced and indices 1 and 2 defines the inflow and outflow of the stream tube. From the energy equation, Eq. (2.15),

assuming adiabatic conditions ($\dot{q} = 0$) one may deduce the following expression for the stagnation temperature

$$\frac{T_0}{T} = 1 + \frac{\gamma - 1}{2} M^2 \tag{2.16}$$

where $M = u/a$ is the *Mach number* and $a = (\gamma R T)^{1/2}$ is the *speed of sound*. Note that T_0 is not a constant for an unsteady flow.

2.2.3. *Streamline flow*

The Bernoulli's principle states that for a constant density fluid, in steady, frictionless flow, the stagnation pressure p_0 is constant along a streamline, and can be expressed as

$$p_0 = p + \frac{1}{2}\rho u^2 = \text{const.} \tag{2.17}$$

Here p is the *static pressure* and $\frac{1}{2}\rho u^2$ is the *dynamic pressure*. It is also possible to express the Bernoulli principle for compressible flow when it takes the form

$$\frac{1}{2}u^2 + \int \frac{dp}{\rho} = \text{const.} \tag{2.18}$$

where the integral should be taken along the streamline. It is readily seen that this expression is equal to the incompressible form if ρ is a constant.

Using the isentropic relationship between T and p (Eq. 2.6) it is easily seen that in compressible flow the ratio between the stagnation and static pressures becomes

$$\frac{p_0}{p} = \left(1 + \frac{\gamma - 1}{2} M^2\right)^{\gamma/(\gamma-1)} \tag{2.19}$$

The right hand side of Eq. (2.19) can be expanded through the binomial theorem such that

$$\begin{aligned} p_0 - p &= \frac{1}{2}\rho u^2 \left[1 + \frac{M^2}{4} + \frac{2 - \gamma}{24} M^4 + \ldots\right] \\ &= \frac{1}{2}\rho u^2 f(M, \gamma) \end{aligned} \tag{2.20}$$

where the bracketed function is sometimes referred to as the *compressibility factor*, which increases with increasing Mach number. At $M = 0$ the incompressible Bernoulli relation Eq. (2.17), is recovered.

2.2.4. *One-dimensional flow with friction*

In many flow systems it is necessary to take friction at the walls into account. In gas-dynamical flow problems it is usual to model the viscous forces in the fluid as a shear stress at the pipe wall, acting on the fluid. Usually this is expressed through a friction factor f which is defined as

$$f = \frac{\tau_w}{\frac{1}{2}\rho u^2} \tag{2.21}$$

The friction factor f is a weak function of the Reynolds number at high Re and is for smooth pipes usually taken as $f = 0.005$.

As a starting point one may assume that the flow is adiabatic and the simple theory assumes that all fluid properties solely vary in the pipe axis direction, and moreover a constant cross section area is assumed.

Since the flow is assumed to be adiabatic and stationary, it implies that T_0=const. Using Eq. (2.16) twice for two locations along the pipe (see Fig. 2.1), we obtain

$$\frac{T_2}{T_1} = \frac{T_0/T_1}{T_0/T_2} = \frac{2 + (\gamma - 1)M_1^2}{2 + (\gamma - 1)M_2^2} \tag{2.22}$$

Now, because the mass flux ρu, is constant for one-dimensional flow, and furthermore having in mind that $u = M\sqrt{\gamma RT}$, the above equation can be expressed in terms of the corresponding pressure ratio

$$\frac{p_2}{p_1} = \frac{M_1}{M_2}\sqrt{\frac{T_2}{T_1}} = \frac{M_1}{M_2}\sqrt{\frac{2 + (\gamma - 1)M_1^2}{2 + (\gamma - 1)M_2^2}} \tag{2.23}$$

Let us assume that the flow at section 2 is sonic, i.e. $M_2 = 1$, the distance between section 1 and 2 is L and the pipe diameter is D, then (for a derivation see e.g. Anderson 2003) it follows that the Mach number at section 1 is a function of the quantity $4fL/D$, viz.

$$\frac{4fL}{D} = \frac{1 - M_1^2}{\gamma M_1^2} + \frac{\gamma + 1}{2\gamma} \ln\left[\frac{(\gamma + 1)M_1^2}{2 + (\gamma - 1)M_1^2}\right] \tag{2.24}$$

This means that the Mach number M_1 can be determined if f, L and D are given, and from this all other ratios between the various flow quantities can be obtained.
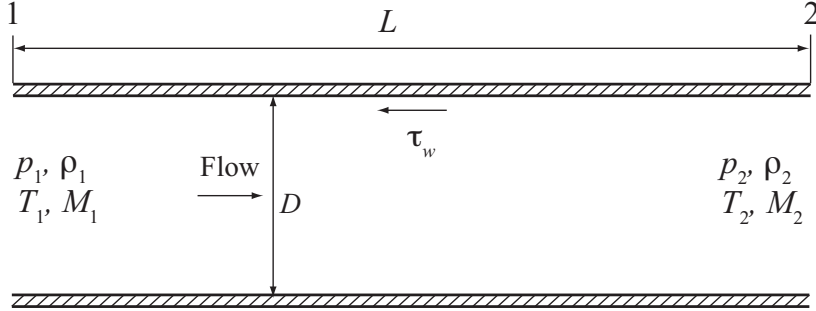

FIGURE 2.1. Pipe section with constant cross section area, for adiabatic one-dimensional flow. The friction is modeled as a shear stress τ_w acting on the fluid from the wall.

2.2.5. *Quasi one-dimensional theory*

If all flow variables just vary with one spatial direction say the x-direction, the flow is said to be one-dimensional. Furthermore, if the cross section area A also varies with spatial direction x, i.e. $A = A(x)$ the flow is said to be quasi one-dimensional. The conservation equations for this case, where we assume that the cross section areas of the stream tube are A_1 and A_2 at the inflow and outflow, respectively, become

$$\rho_1 u_1 A_1 = \rho_2 u_2 A_2 \tag{2.25}$$

$$p_1 A_1 + \rho_1 u_1^2 A_1 = p_2 A_2 + \rho_2 u_2^2 A_2 - \int_{S_{\text{lat}}} (\rho \mathbf{u} \cdot d\mathbf{S}) \mathbf{u} \tag{2.26}$$

$$h_1 + \frac{1}{2} u_1^2 = h_2 + \frac{1}{2} u_2^2 + \dot{q} \tag{2.27}$$

The change in the mass conservation equation is readily seen, in the momentum conservation there will be a contribution from the pressure on the lateral area (S_{lat}) of the control volume, whereas the energy equation does not change with respect to the 1-D case.

In the following some basic quasi one-dimensional relations will be described.

From the mass conservation equation in quasi one-dimensional flow, Eq. (2.25), at two locations along e.g. a *nozzle* (see Fig. 2.2), one can relate the Mach numbers and cross section areas according to

$$\left(\frac{A_1}{A_2}\right)^2 = \left(\frac{M_2}{M_1}\right)^2 \left(\frac{1 + \dfrac{\gamma - 1}{2} M_1^2}{1 + \dfrac{\gamma - 1}{2} M_2^2}\right)^{(\gamma+1)/(\gamma-1)} \tag{2.28}$$

where the flow between section 1 and 2 is assumed to be isentropic. The second parenthesis on the right hand side in the above relation can be expressed by means of the pressure ratio p_2/p_1 since

$$\frac{p_2}{p_1} = \frac{p_2/p_0}{p_1/p_0} = \left(\frac{1 + \dfrac{\gamma - 1}{2} M_1^2}{1 + \dfrac{\gamma - 1}{2} M_2^2}\right)^{\gamma/(\gamma-1)} \tag{2.29}$$

Moreover, if M_2 is eliminated through Eq. (2.19) and using that $\dfrac{p_0}{p_2} = \dfrac{p_0}{p_1} \dfrac{p_1}{p_2}$, where $\dfrac{p_0}{p_1}$ can be expressed as a function of M_1 through Eq. (2.19), it is possible to express the Mach number at location 1 in terms of the area and pressure ratio alone

$$M_1^2 = \frac{2}{\gamma - 1} \left[1 - \left(\frac{p_2}{p_1}\right)^{(\gamma-1)/\gamma} \right] \left[\left(\frac{A_1}{A_2}\right)^2 \left(\frac{p_2}{p_1}\right)^{-2/\gamma} - 1 \right]^{-1} \tag{2.30}$$

Now assume that we are studying the flow in a nozzle, such as the one in Fig. 2.2. If the pressure difference between the inlet and the outlet of the nozzle is gradually increased, the Mach number at the throat section of the nozzle, will ultimately reach unity. When this happens, the flow is said to be *choked*, and the mass flow rate will stay constant, regardless if the pressure difference is further increased. In fact, the mass flow rate essentially becomes a linear function of the stagnation pressure. If the the quantities at the throat at sonic conditions are denoted with an asterisk, one has $\dot{m} = \rho^* A^* a^*$ and hence

$$
\begin{aligned}
\dot{m} &= \frac{\rho^*}{\rho_0} \rho_0 A^* \frac{a^*}{a_0} a_0 \\
&= \frac{p_0 A^*}{\sqrt{RT_0}} \sqrt{\gamma} \frac{\rho^*}{\rho_0} \sqrt{\frac{T^*}{T_0}}
\end{aligned}
\tag{2.31}
$$

In the above relation, the ratios ρ^*/ρ_0 and T^*/T_0 are simply constants since they only depend on M^*, which is equal to one, if the flow is choked. Insertion of these constants in Eq. (2.31), results in the expression for the mass flow through a choked nozzle

$$
\dot{m} = \frac{p_0 A^*}{\sqrt{RT_0}} \sqrt{\gamma \left(\frac{2}{\gamma+1} \right)^{(\gamma+1)/(\gamma-1)}}
\tag{2.32}
$$

where the square root term is for a gas with $\gamma = 1.40$, equal to 0.685.
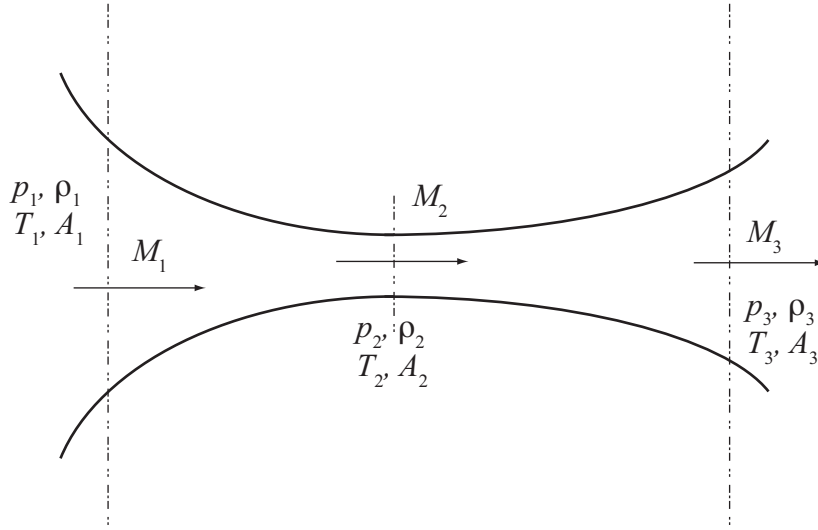

FIGURE 2.2. *Convergent-divergent nozzle.* For high enough pressure ratio p_1/p_3, the flow becomes choked, and at section 2 the sonic speed is obtained.

CHAPTER 3

Flow measuring techniques

Flow measuring occurs in many different places, such as industry, for domestic purposes, in hospitals for medical applications and in research laboratories, just to name a few. Depending on ones preferences regarding flow meters, such as desired accuracy, measuring range, costs etc., there are a vast number of flow measurement techniques available to choose between. The intention with this chapter is to account for some of the more commonly used flow meters in both industry and in fluid mechanics laboratories that can be used to measure mass flow rate. There exists an immense amount of literature in this field, so a complete elaboration would be superfluous.

For liquids it is usually equivalent to measure volume flow or mass flow since they can be simply related if the density of the fluid is known. For gas flows volumetric measurements does not make sense when being in the compressible region, since for a compressible fluid the volume flow rate depends on the pressure. This chapter focusses on methods that are employed to measure flow rates in compressible flows. Also some techniques that are usually used for incompressible flows are discussed and their potential to be used also in compressible flow situations are discussed. The dynamic response, i.e. the meters ability to measure correct average values in pulsating flows, is also discussed, but also if the flow meter is able to resolve the pulsating flow rate. The objective of the present work is to evaluate and develop flow measuring methods that can be used in the range of typical internal combustion engine flows. For the present work we focus on pulsating flows up to 80 Hz pulse frequency and mass flow rates up to about 200 g/s. The general principle of the flow meter in question will be described, followed by its dynamic characteristics.

Flow meters can in principal be divided into four distinctive groups (cf. Omega 1995) depending on how the flow rate is obtained. These are: *differential pressure flow meters*, *mechanical flow meters*, *electronic flow meters* and *mass flow meters*. Nevertheless, common for all of these meters is that they are designed to measure the *bulk flow*, i.e. the volume or mass of fluid, flowing through some sort of flow conduit, per unit time (volume flow rate Q and mass flow rate $\dot{m}$ respectively). In the following we will describe various flow meter techniques under these headings.

3.1. Differential pressure flow meters

The perhaps most commonly employed method in both industry and fluid mechanics laboratories to obtain flow rates, is the measurement of the pressure drop across a pipe restriction, known as *differential pressure flow meters*. A subgroup of these are the so called *restriction flow meters*, that includes *orifice plate*, *venturi* and *nozzle* which will be described in the subsequent text. The principle for these devices is that the flow is accelerated through a restriction, thus creating a decrease in static pressure. The flow rate is in turn estimated from measurements of the induced pressure difference.

3.1.1. *Restriction flow meters*

For restriction flow meters various standards, such as ISO and ASME standards, are available, which give the possibility to use such meters without calibration. However there are certain limitations on the operating range, such as the maximum pressure ratio over the device. For even higher pressure ratios a restriction flow meter may choke and this places other limitations on the meter. For a pulsating flow this may mean that during high flow rates the meter may work under choked conditions, although the mean flow rate would imply non-choked flow.

3.1.1a. *Orifice plate.* An orifice plate is essentially a thin plate with a centered hole, mounted in a pipe, as illustrated in Fig. 3.1. Two static pressure taps are located on each side of the plate.

First let us consider steady, incompressible flow without dissipation of energy in a stream tube. Then, the drop in pressure is related to the flow speed by the Bernoulli's equation, Eq. (2.17) and the relation between the velocities is yielded from continuity, for a constant density fluid, Eq. (2.10). These two relations may be combined to give
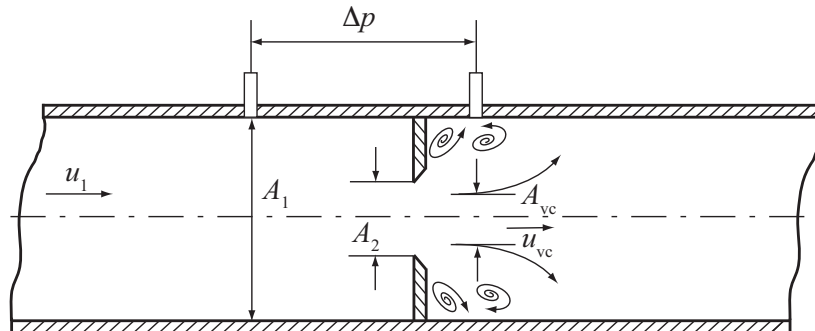

FIGURE 3.1. *Orifice plate.* The downstream pressure should be measured at the *vena contracta.*

$$
\begin{aligned}
Q &= A_2\sqrt{\frac{2(p_1 - p_2)/\rho}{1 - (A_2/A_1)^2}} \\
&= A_2\sqrt{\frac{2\Delta p/\rho}{1 - (d_2/d_1)^4}}
\end{aligned}
\tag{3.1}
$$

where index 1 denotes the station upstream the plate and 2 is at the *vena contracta*[1]. Hence, Eq. (3.1) describes the idealized flow rate. However for an orifice plate the *vena contracta* has not the same diameter as the diameter of the hole in orifice plate and therefore a coefficient of discharge C_d must be introduced. C_d is the ratio of the actual flow rate to the idealized flow rate, now Eq. (3.1) turn into

$$
Q = C_d A_2\sqrt{\frac{2\Delta p/\rho}{1 - (d_2/d_1)^4}}
\tag{3.2}
$$

The *coefficient of discharge* is around 0.6 and varies slightly with the Reynolds number Re, which is the ratio of inertial to viscous forces

$$
\mathrm{Re} = \frac{\rho u d}{\mu}
\tag{3.3}
$$

where d is a, for the problem, characteristic length, (e.g. the pipe diameter in pipe flow) and μ is the dynamic viscosity of the fluid.

In the case of compressible flow Eq. (3.2) may be further modified to include a correction in terms of the expansibility factor ε_1, to become

$$
Q = C_d \varepsilon_1 A_2\sqrt{\frac{2\Delta p/\rho_1}{1 - (d_2/d_1)^4}}
\tag{3.4}
$$

or expressed in terms of mass flow rate, rather than volume flow rate

$$
\dot{m} = \rho_1 Q_1 = C_d \varepsilon_1 A_2\sqrt{\frac{2\Delta p \rho_1}{1 - (d_2/d_1)^4}}
\tag{3.5}
$$

The expansibility factor ε_1 is a function of the Reynolds number, the pressure ratio p_2/p_1 and the ratio between specific heats for the gas considered and is < 1. According to standard practice[2] this procedure is only valid if the pressure ratio $p_2/p_1 > 0.75$.

---

[1] The *vena contracta* is a contraction in the flow, situated downstream an orifice. The location is not fixed, but depends on the flow conditions.
[2] Data for e.g. ε_1 and C_d can for instance be obtained from ISO-5167 (2003).

3.1.1b. *Venturi flow meter.* This flow meter device is based on the same principle as the orifice plate, thus the derivation of the flow rate equation, will be quite analogous to Eqs. (3.1) through (3.5). The device consists of one short converging part, a throat and a longer diverging part (Fig. 3.2). The main difference compared to the orifice plate is that the pressure drop across the flow meter is much smaller, because separation does not occur in the diverging part, if the angle θ is sufficiently small. The larger the angle, the larger the adverse pressure gradient, which if too large may lead to separation.

In order to measure the flow rate in the venturi flow meter in a more direct way it is possible to use the compressible gas dynamics equations. In that case one can relate the upstream and downstream pressures to the Mach numbers at the corresponding sections. By knowing the area ratios it is possible to use standard compressible flow equations to obtain a good approximation of the mass flow rate. The details of this procedure is further developed in Sec. 5.2.
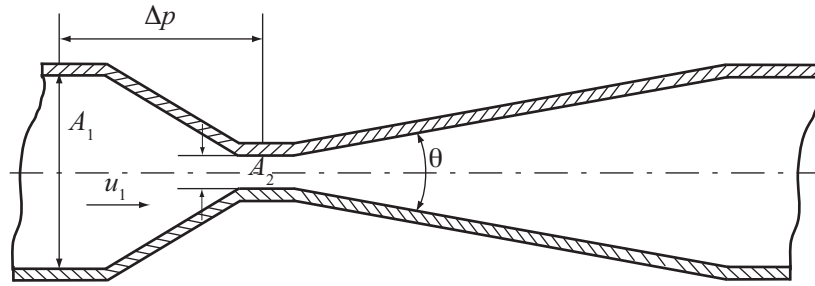

FIGURE 3.2. *Venturi flow meter.* The θ angle should be about $6°$ (or less) to avoid separation.

3.1.1c. *Nozzle.* If pressure losses are considered, the *flow nozzle* can be regarded as something in between the two aforementioned restriction flow meters. It has not as good pressure recovery as the venturi, but better than the orifice plate. The downstream end of the flow nozzle, depicted in Fig. 3.3, consists of a tube with the same diameter as the vena contracta of an equivalent orifice plate.

For a certain ratio of the pressure upstream and downstream the flow nozzle, the velocity in the throat becomes sonic. This is as mentioned previously called *choked flow*, and these so called critical flow nozzles can be used as very accurate flow meters, where only the stagnation conditions of the gas (for instance the stagnation pressure and temperature) upstream the nozzle have to be determined accurately, in order to obtain the flow rate.
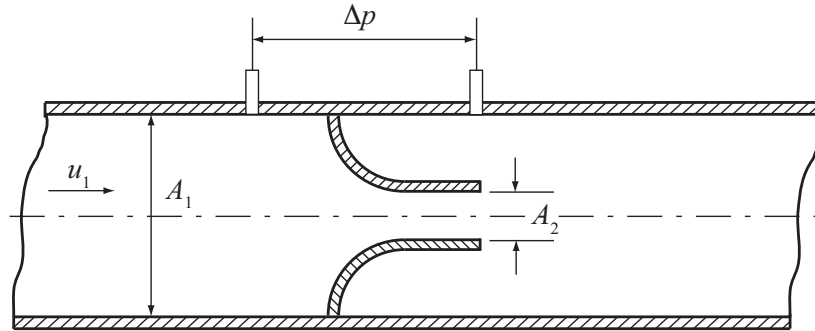
FIGURE 3.3. *Nozzle.* The downstream pressure tap should be mounted inside the nozzle exit.

3.1.1d. *Dynamic behavior.* Several error sources are associated with measurements using restriction flow meters in pulsating flows. One such error source that can arise concerns the pressure transducer set-up. For steady flow measurements, it is practical to use a differential pressure transducer to measure the pressure difference over the flow meter and the time response of the pressure transducer is not critical. However, in pulsating flows this may lead to long lag times in the tubing, which may give erroneous readings of the instantaneous pressure difference. To be able to resolve the pulsating flow, it is therefore necessary to use flush mounted absolute pressure transducers. It is then, however, important to have a good calibration of these transducers.

As discussed in Gajan *et al.* (1992), the probably most frequently error in the flow rate estimation emanates from the square root relationship with flow rate, i.e. if the average of pressure is taken before the the square root operation, one get an overestimate of the flow rate. This is illustrated in Fig. 3.4, as inspired by the work of Nakamura *et al.* (2005). In Fig. 3.4 a time varying velocity (represented by a sine) is transformed into the pressure domain, where the aforementioned error in velocity is denoted by $\Delta u_{\mathrm{error}}$. The conclusion one can draw from this, is that it is important to calculate the square root of the pressure difference at each instant of time. In general, it is necessary for each instant of time to calculate the quantity desired, which in this case is the velocity.
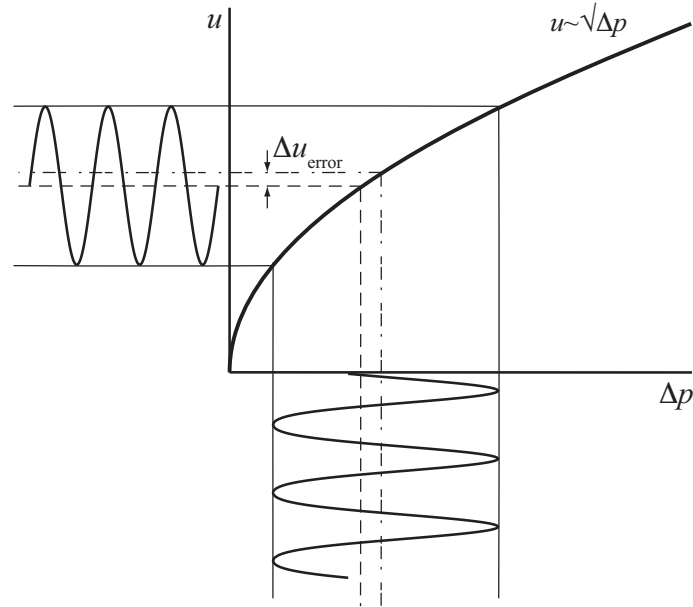
FIGURE 3.4. Illustration of the square root error. The dashed line is the mean taken in the velocity domain, whereas the dash-dotted line is the mean taken in the pressure domain. As can be seen from the illustration, making the the square root operation after averaging the pressure, can give rise to large overestimation in velocity.

3.1.2. *Laminar flow elements*

Laminar flow meters are usually pipe sections that contains some sort of honeycombs, schematically illustrated in Fig. 3.5. Inside the honeycomb the flow is laminar, passing through narrow channels in the honeycomb, so that the Reynolds number is below the transitional value of $Re \approx 2300$. The volume flow rate for this device, is given by the Hagen-Poiseuille formula (see e.g. Massey & Ward-Smith 1998), which for a pipe section of length Δx and diameter D becomes

$$Q = \frac{\pi D^4}{128\mu} \frac{\Delta p}{\Delta x} \tag{3.6}$$

The derivation of this relation is straightforward. Consider a cylinder of radius r, the force balance of the cylinder of radius r is $p\pi r^2 - (p + \delta p)\pi r^2 + \tau_w 2\pi r \delta x = 0$, where τ_w is the wall shear stress. Thus for small δx, the wall
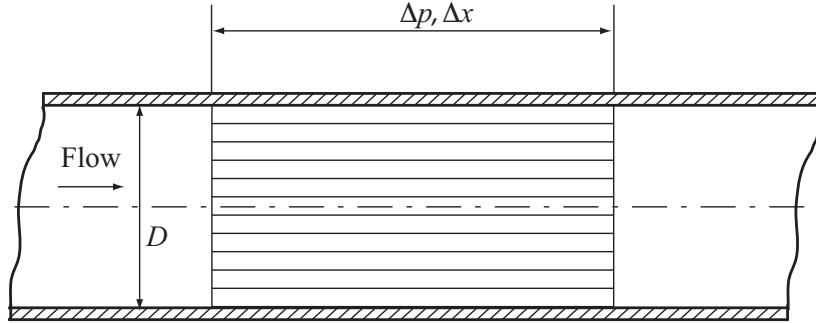
FIGURE 3.5. *Laminar flow element.* The Honeycomb straightens the flow up and makes it laminar, due to the narrow channels.

shear stress becomes

$$\tau_w = \frac{r}{2}\frac{dp}{dx} \tag{3.7}$$

Now the wall shear stress is obtained from

$$\tau_w = \mu\frac{\partial u}{\partial r} \tag{3.8}$$

Because the velocity only varies with r, we have that

$$\mu\frac{du}{dr} = \frac{r}{2}\frac{dp}{dx} \tag{3.9}$$

Which, if μ is constant, can be integrated to yield

$$u = -\frac{1}{4\mu}\frac{dp}{dx}(R^2 - r^2) \tag{3.10}$$

where the constant of integration is obtained by applying the no slip boundary condition $u(R) = 0$. The volume flow rate in small annular area is

$$\begin{aligned}\delta Q &= u\delta A = u2\pi r\delta r \\ &= -\frac{\pi}{2\mu}\frac{dp}{dx}(R^2 r - r^3)\delta r \end{aligned} \tag{3.11}$$

This can be integrated through the whole cross-section to get

$$Q = -\frac{\pi D^4}{128\mu}\frac{dp}{dx} \tag{3.12}$$

So, for a pipe of length Δx and a pressure drop of $\Delta p = p_1 - p_2$, expressing Eq. (3.12) in terms of diameter D, we finally end up with Eq. (3.6). It should however be emphasized that Eq. (3.12) is valid for both compressible and incompressible fluids since it only considers an infinitesimal length of the pipe. Eq. (3.6) is an integration over the full honeycomb which means that one expects the flow to be incompressible.

3.1.3. *Pitot tube meters*

In its most simple form, the *Pitot tube* measures the stagnation pressure p_0 at a point in the flow field. However, in order to obtain the velocity of the fluid, the static pressure must also be measured. This can be done at the pipe wall, at the same cross section as the tip of the Pitot tube is immersed in the flow (see Fig. 3.6(a)). Another possibility is to use a Pitot static tube (sometimes referred to as a *Prandtl tube*), where both stagnation and static pressure holes are situated in the same device. Note that both these devices make point measurements.

When the average velocity of the flow, rather than the velocity in a specific point in the cross section is desired, a so called *Averaging pitot tube*, can be employed (see Fig. 3.6(b)). This method assumes a turbulent flow profile and the holes are distributed in such a way that they are assumed to give a good estimate of the bulk flow rate. It is however argued whether the Averaging Pitot tube is measuring the true mean flow rate. Baker (2000) claims that the averaging Pitot tube is unlikely to provide a true average of the axial velocities across the pipe. He further suggests that if the velocity is measured at a point where $r = 0.758R$ for fully developed turbulent pipe flow, the velocity at that point will be close to the mean velocity. An approximate curve fit for turbulent pipe flow is

$$u = u_0(1 - r/R)^{1/n} \tag{3.13}$$

where u_0 is the centerline velocity and n depends on Re. From experiments it has been found to vary in the range $6 < n < 10$, with a increasing value for increasing Re. The ratio of the local to the bulk velocity is thus given by

$$\frac{u}{u_b} = \frac{(n+1)(2n+1)}{2n^2}(1 - r/R)^{1/n} \tag{3.14}$$

The deviation from the mean velocity is less than 0.2 % for n between 6 and 10 at the location $r = 0.758R$.

Assuming incompressible flow, the volume flow rate can be obtained directly from Bernouilli's equation, since the velocity is reduced to zero at the tip of the Pitot tube, and thereby it measures the stagnation pressure. Moreover, assuming the Pitot tube provides a proper estimation of the bulk velocity we obtain

$$Q = \frac{\pi D^2}{4}\sqrt{\frac{2\Delta p}{\rho}} \tag{3.15}$$

where $\Delta p = p_0 - p$. This expression may be corrected for compressibility effects, however, if the Mach number becomes large it may be better to use the correct equations for isentropic flow discussed in Chap. 2 and especially Eq. (2.19). This equation can be expanded (Eq. (2.20) repeated here again) to yield

(a)

(b)
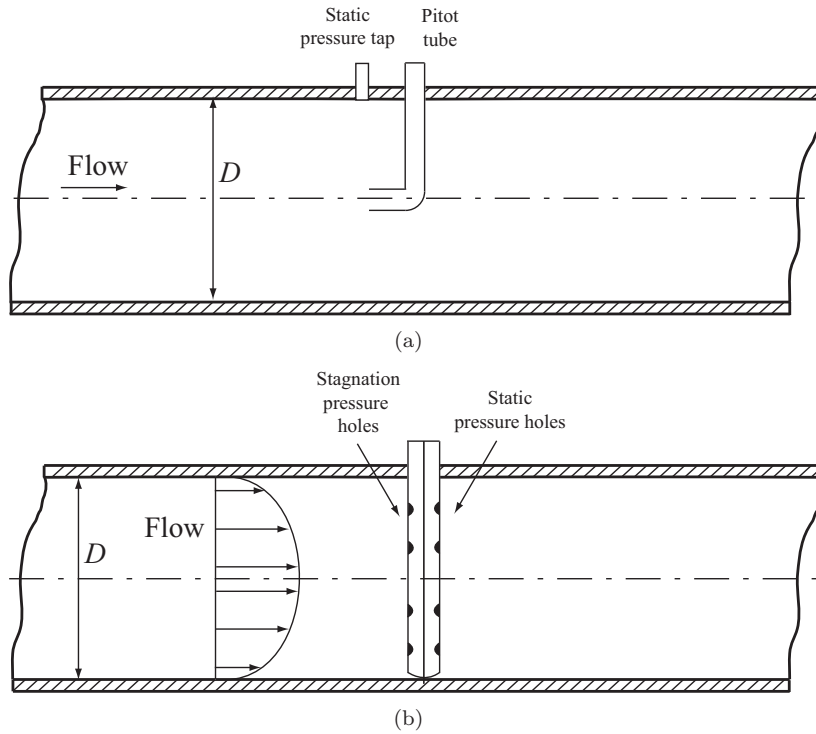
FIGURE 3.6. (a) *Pitot tube.* (b) *Averaging Pitot tube.*

$$p_0 = p + \frac{1}{2}\rho u^2 \left[1 + \frac{1}{4}M^2 + \ldots\right] \tag{3.16}$$

The second term within the parenthesis is the correction term which shows the contribution due to compressibility. If this expression is introduced in Eq. (3.15) one observes that for $M = 0.3$ the flow rate is underestimated with about 1% and at $M = 0.5$ with 3%.

3.1.3a. *Dynamic behavior.* If a Pitot tube is used to obtain time resolved measurements it is necessary to reduce the tubing length to the pressure transducer. Nakamura *et al.* (2005) measured pulsating gas from an engine exhaust using an averaging Pitot tube. It was concluded that the Pitot tube needs to be combined with a fast response differential pressure transducer. This resulted in a good correlation with reference flow measurement devices. Furthermore they showed that the pulsations could cause a maximum of five times higher errors, owing to the averaging procedure, i.e. if the averaging is done in the

pressure domain or the flow rate domain, as discussed in the orifice plate section. Another way to obtain the instantaneous pressure difference is to use two separate absolute pressure transducers connected to the Pitot tube and the static pressure respectively, and thereafter use the pressure ratio to obtain the velocity (and hence also the flow rate). In this way one also automatically obtains the pressure so that the density can be determined (if also the temperature is known) and thereby the mass flow rate.

3.2. Mechanical flow meters

3.2.1. *Turbine flow meter*

A *turbine flow meter* consists of an immersed vaned rotor in a pipe section. The most common type has a rotor which is made to rotate along an axis in the flow direction, and if well designed, it will give a linear relationship between the volume flow rate and the rotational speed of the turbine (see Fig. 3.7). The frequency of the rotor is usually sensed electromagnetically by an external sensor. The volume flow rate Q is not measured directly, but is related to the frequency f of the rotor which is driven by the flow. The relation is simply (see for instance Merzkirch 2005)

$$f = kQ \tag{3.17}$$

where the so called k-factor depends on the geometry of the turbine. Turbine flow meters are usually used for liquids, i.e. fluids that are incompressible, however they can also be used for gases. In order to determine the mass flow rate one has to estimate the density of the gas, and one possibility is to determine it from the average pressure upstream and downstream of the turbine.
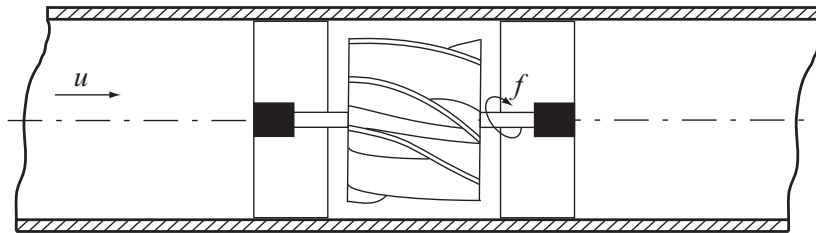

FIGURE 3.7. *Turbine flow meter.* This is an axial turbine blade design, although different blade designs are possible.

3.2.1a. *Dynamic behavior.* A well known issue with the turbine flow meter, regarding pulsating flow, is that they usually tend to overestimate the flow rate. This was e.g. demonstrated by McKee (1992), who showed that pulsating flow has a distinct influence on the overestimation of the flow rate. This influence is depends upon the physical design of the turbine meter but also upon the flow conditions, such as flow rate, density, pulsating frequency and amplitude.

3.2.2. *Rotameter*

The *Rotameter* is the most frequent example of a *variable area meter*, due to its versatility and simplicity. A floating body is immersed in a conical tube as illustrated in Fig. 3.8. The flow enters the lower end of the tube and exits at the upper end. The floating body rises in the conical tube, because of the

flow induced drag. In turn, this force is balanced by the gravity and buoyancy forces. However, in the case of gas flow, the buoyancy force will be insignificant.

The flow rate Q will be linearly proportional to the height y. To appreciate this, note that the annular area between the body and the tube wall A is approximately linearly related to the height, i.e. $A \sim y$. Furthermore, the drag F_d should balance the the body weight and is hence independent of the flow rate, thus $F_d = \text{const}$. This implies that $F_d \sim \rho u^2 \sim \rho(Q/A)^2$. Accordingly we obtain

$$Q \sim y \tag{3.18}$$

(provided that ρ can be considered as constant). The height of the floating body can for instance be read manually or sensed by an electromagnetic device. As can be seen also the density of the fluid comes into play, so this type of device is mainly useful for constant density fluids.
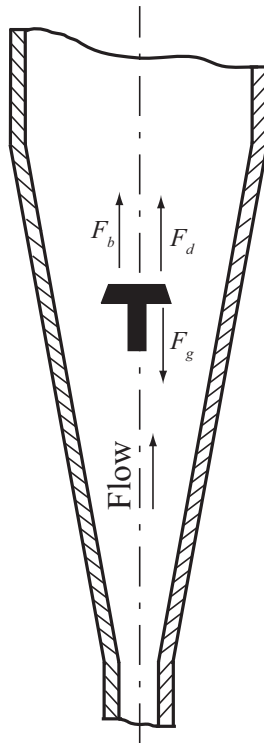

FIGURE 3.8. *Rotameter.* The drag force F_d, on the float body is balanced by the difference between the gravitational force F_g and the buoyancy force F_b.

3.3. Vortex shedding flow meter

The *vortex-shedding flow meter* is based on the principle of periodic separation of flow behind an obstruction (*von Karman vortex street*). The flow detaches from sharp edges of the obstruction, periodically at a frequency f, as depicted in Fig. 3.9. The main feature of this phenomenon is that the dimensionless frequency of the shedding, the so called *Strouhal number*, is constant, i.e. independent of u for a large range of Re, (see for example Kundu & Cohen 2004). The Strouhal number is given by

$$\text{St} = \frac{fd}{u} \tag{3.19}$$

where d is some characteristic cross stream length of the obstruction. Provided that the flow profile is decently uniform, the frequency f, will be proportional to the flow velocity u. The shedding frequency can be obtained with different kind of methods like measuring frequency of pressure fluctuations or the impact on the body with strain gauges. If a vortex shedding meter should be used to measure mass flow rate in a gas flow one also has to provide separately a measure of the fluid density by measuring the pressure and temperature of the gas at the position of the flow meter.
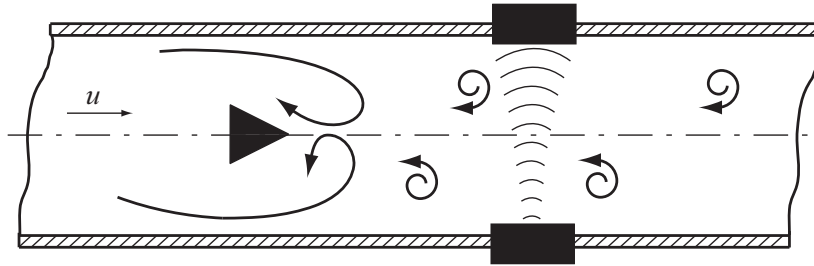
FIGURE 3.9. *Vortex flow meter*. The separation of flow past the bluff body is occurring alternating on each side of it, with a frequency proportional to the flow velocity.

3.3.1. *Dynamic behavior*

As concluded by Hebrard *et al.* (1992), even low amplitude pulsations can be sufficient to obtain metering errors of the flow rate. This is especially visible when the frequency of pulsation is near the fundamental vortex shedding frequency. For further elaboration in this matter, the reader is referred to Laurantzon *et al.* (2010*b*), Paper 3.

3.4. Mass flow meters

3.4.1. *Coriolis flow meter*

A *Coriolis flow meter* consists of a flow tube which is subject to vibrations by means of e.g. an alternating magnetic field (see for example Tavoularis 2005). Although the meters design can vary widely, the principle is the same for all of them, namely the Coriolis force principle. Consider a fluid packet with mass δm, with velocity u, see Fig. 3.10 (a). If the tube is oscillating with an angular frequency ω, about an axis normal to the axis of the tube and the packet is situated a distance r from the axis of rotation, the packet has an angular momentum $H = \delta m \omega r^2$. Now if the packet is displaced by a distance δr in time $\delta t = \delta r / u$ from this position, it has an angular momentum $H = \delta m \omega (r + \delta r)^2 \approx \delta m \omega (r + 2r\delta r)$. The change in angular momentum is accordingly $\delta H = 2\delta m \omega r \delta r$. The time rate of change of the angular momentum is the torque done by the fluid, i.e. $\delta H / \delta t = 2r\delta m \omega u = F_c r$. From the last equality we identify the force giving rise to the torque as the Coriolis force

$$F_c = 2\delta m u \omega \tag{3.20}$$

Because $\delta m = \rho A \delta x$, for constant cross sectional area A, and using the expression for the mass flow rate ($\rho A u$), we end up with

$$\dot{m} = \frac{F_c}{2\omega \delta x} \tag{3.21}$$

A common flow tube design is the U-tube Coriolis flow meter, Fig. 3.10 (b), where the flow enters and passes a tube bend. The device is set to oscillate at the tubes eigenfrequency. Since the eigenfrequency is dependent of the mass of the tube plus the portion of fluid inside the tube, it is possible to determine the density ρ of the fluid, by comparing the departure in eigenfrequency with e.g. an empty tube. Due to the Coriolis force, the two legs of the tube will suffer a force in opposite directions. Thus, the tubes will be twisted in two ways during one period, owing to the sign of the angular velocity. The twist amplitude of the tube can be sensed by for instance magnetic sensors, and this amplitude will be proportional to the mass flow rate.

3.4.1a. *Dynamic response.* The Coriolis flow meters response to pulsating flow is studied in Cheesewright & Clark (1998), where they found that a true mean mass flow rate could be obtained also in pulsating flow, if the processing of the detector signals where done in an appropriate way. Furthermore, Vetter & Notzon (1994) found that Coriolis flowmeters can give erroneous output if the frequency of the flow pulsations and the Coriolis meter frequency coincide.
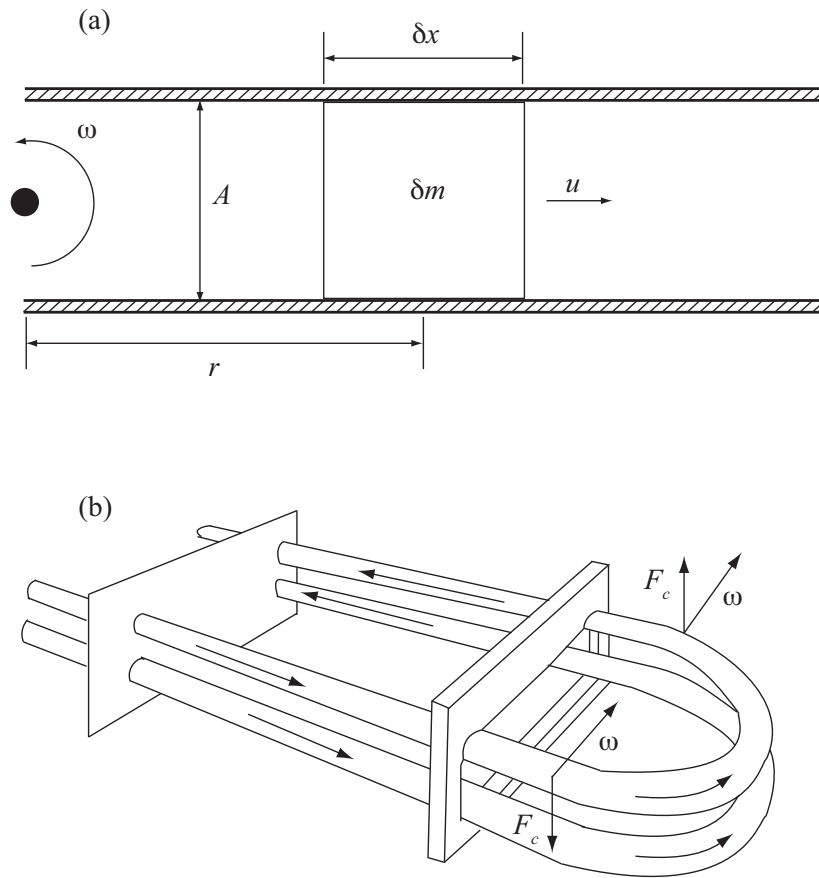
(a)

(b)

FIGURE 3.10. *Coriolis flow meter.* (a) A fluid packet with mass δm and velocity u in a pipe section. (b) The common U-tube design.

3.4.2. *Corona mass flow meter*

The *corona mass flow meter* CMFM, relies on the transport of ions in an electrical field. The ions are created by a thin metal wire or a pointed tip that is held at a high voltage (~ 10 kV, for a wire with with a radius of $25\ \mu$m). Corona wires are widely used in various technical applications such as photocopiers and electrostatic precipitators. The geometry used for a corona mass flow meter may vary. A common design is shown in Fig. 3.11. This design of the meter is a coaxial arrangement with two outer grounded metallic cylinders (cathodes) and an inner, thin metal wire (anode) with radius a. When applying a high (positive) direct current voltage to the wire, natural free electrons are

accelerated towards the wire and at high enough speeds collisions between electrons and gas molecules give rise to ionized molecules and new electrons. The wire is mounted concentrically with two identical outer hollow cylindrical electrodes which are located along the inner pipe wall. The electrodes are axially separated by a couple of millimeters. When the potential of the wire is sufficiently large, the gas around and close to the thin center wire will ionize and positive ions are attracted to the two wall electrodes (for a more thorough review regarding the physics, consult e.g. Chen & Davidson 2002). This sets up a current between the outer two electrodes and the ground, i_1 and i_2, respectively.
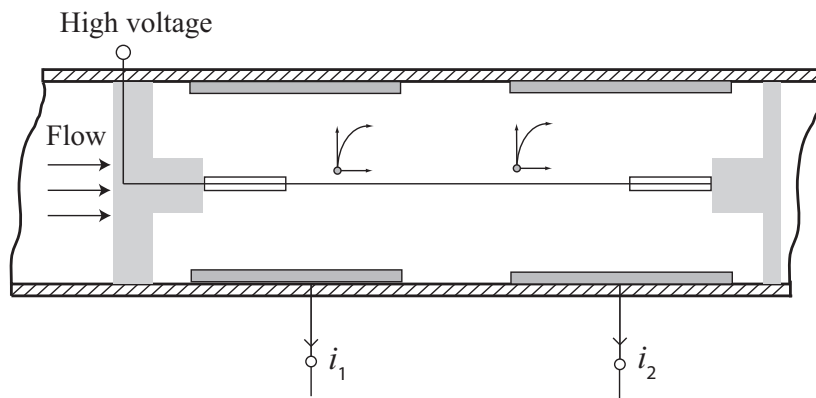

FIGURE 3.11. *Corona mass flow meter.* Ions deflect more or less to either electrode, depending on the mass flow rate.

When gas is flowing through the mass flow meter, the number of ions that reaches the downstream electrode will be larger than for the upstream electrode, thereby making $i_2 > i_1$. A CMFM with the design as in Fig. 3.11 is described in Laurantzon *et al.* (2008), Paper 1. Here, each wall electrode is connected to a precision resistor which both have the same resistance R. The voltage potential difference ($\Delta V = V_2 - V_1$) between the top of both resistors is then related to the difference in currents ($\Delta i = i_2 - i_1$) through the two wall electrodes as $\Delta i = \Delta V / R$. The output from the CMFM depends on several geometrical and physical parameters. Obviously the voltage applied to the the corona wire has to be high enough for the corona to form and if the corona is formed the current density will increase with increasing voltage potential at the wire.

3.4.2a. *Dynamic response.* It is obvious from the previous description that if the flow is reversed then also the output will change sign. This is an important feature when measuring pulsating flow, since a back flow is then directly

detected. For the frequency response of the CMFM the length (L) and diameter (D) of the cathodes and their axial separation (Δ) may be important or rather the non-dimensional parameters (L/D) and Δ/L. In Laurantzon *et al.* (2008), Paper 1, a few measurements in pulsating flow were conducted, however no firm conclusions regarding its potential to handle pulsating flow, could be drawn from these measurements. Hence, the potential to use the CMFM in pulsating flows needs to be further investigated. Also the design needs to be optimized for such measurements.

3.4.3. *Thermal mass flow meter*

Thermal mass flow meters exists in two types, as discussed in Tavoularis (2005), namely the *heated-tube flow meter* and the *immersion-probe flow meter*. The former operates by means of supplying a known amount of heat $\dot{q}$ into the flow device and measure the temperature change upstream and downstream the device. The mass flow rate is then related to the temperature difference ΔT according to

$$\dot{m} = \frac{\dot{q}}{c_p \Delta T} \tag{3.22}$$

Because of relative high values of the specific heat c_p for liquids, this measuring method is only suitable for gases, but will not be discussed further here.

On the other hand, the *immersion-probe flow meter* is based on the fact that an object immersed in a flow stream is cooled down. This is used for the two common sensor types, *hot-wire* and *hot-film* respectively, which are commonly used in engine applications. Both methods are based on convective heat transfer from a heated element, at a temperature above the ambient, placed in the flow. However, in comparison, the hot wire has better frequency response than the hot film, whereas the hot film better can withstand contamination. The heat transfer mechanism is similar for both hot wire and hot film, and so the subsequent analysis will be applicable for both sensor types.

3.4.3a. *Heat transfer from a hot-wire sensor.* Consider a wire, heated to some temperature T_w. The rate of heat transferred to the surroundings by forced convection is according to *Newton's law of cooling*

$$\frac{dQ}{dt} = I^2 R_\mathrm{w} = h A_\mathrm{w} (T_\mathrm{w} - T_\mathrm{f}) \tag{3.23}$$

where R_w, A_w and T_w is the resistance, the projected area and the temperature of the wire respectively, T_f is the ambient fluid temperature, h is the convective heat transfer coefficient and finally, I is the electrical current through the wire, which through resistive (ohmic) heating heats the sensor. In the linear approximation, valid for common hot-wire operational conditions, the resistance of the wire varies with temperature according to

$$R_\mathrm{w} = R_\mathrm{ref}[1 + \alpha_\mathrm{ref}(T_\mathrm{w} - T_\mathrm{ref})] \tag{3.24}$$

Here, R_{ref} is the resistance at the reference temperature T_{ref}, which typically is room temperature. Furthermore, the temperature coefficient of resistivity α_{ref}, depends on the wire material[3].

Introducing the ratio of convective to conductive heat transfer coefficients the non dimensional Nusselt number

$$\mathrm{Nu} = h\ell/k_f \tag{3.25}$$

can be formed, where k_f is the thermal conductivity of the fluid and ℓ a characteristic length. For a compressible fluid, Nu depends on several parameters and can be written as

$$\mathrm{Nu} = \mathrm{Nu}(\mathrm{Re}, \mathrm{Pr}, M, T_{\mathrm{w}}, T_0, T_{\mathrm{r}}, \ell/D) \tag{3.26}$$

where Pr is the Prandtl number, T_{r} is the recovery temperature and ℓ/D is the length to diameter ratio for the wire. If the definition of the Nusselt number is employed in Eq. (3.23), it becomes

$$I^2 R_{\mathrm{w}} = k_{\mathrm{f}} \mathrm{Nu} \frac{A_{\mathrm{w}}}{\ell}(T_{\mathrm{w}} - T_{\mathrm{f}}) \tag{3.27}$$

Moreover, following the discussion in Bruun (1995), it can be shown that

$$\mathrm{Nu} = A_1 + B_1 \mathrm{Re}^n = A_2 + B_2(\rho u)^n \tag{3.28}$$

(where of course $A_1 = A_2$). Furthermore, using Ohm's law ($E = R_{\mathrm{w}}I$), we consequently obtain

$$\begin{aligned} E^2 = & (A_3 + B_3(\rho u)^n)(T_{\mathrm{w}} - T_{\mathrm{f}}) \\ = & A(T) + B(T)(\rho u)^n \end{aligned} \tag{3.29}$$

For a constant density fluid, ρ can of course be absorbed in the definition of B. The above relation was first deduced by King (1914) and we shall henceforth refer to it as "King's law". The coefficients A and B are functions of the both the fluid and sensor temperature and has to be calibrated for each specific set-up. The exponent n is for most applications usually about 0.5[4].

Thus there is a non-linear relationship between the anemometer output voltage and the mass flux. Analogous to the aforementioned problem with the square root error for differential pressure devices, the non-linear relation between velocity and voltage, $u \sim E^4$, yields the opposite problem. Hence, an average done in the voltage domain instead of the velocity domain, gives an underestimation of the velocity, as illustrated in Fig. 3.12. Furthermore, one can see that for fluctuations at low velocities, the change in the voltage is quite large, thus the hot-wire technique has its largest sensitivity at low velocities, which is opposite to that of differential pressure devices.

---

[3]For most metals used the value of α is around 0.003 ± 0.001 K^{-1}, in the temperature range of interest.

[4]King (1914) showed that n theoretically should be equal to 0.5 for an infinitely long wire. For a hot-wire sensor n is usually determined together with the constants A and B through a least square fit to experimental data.
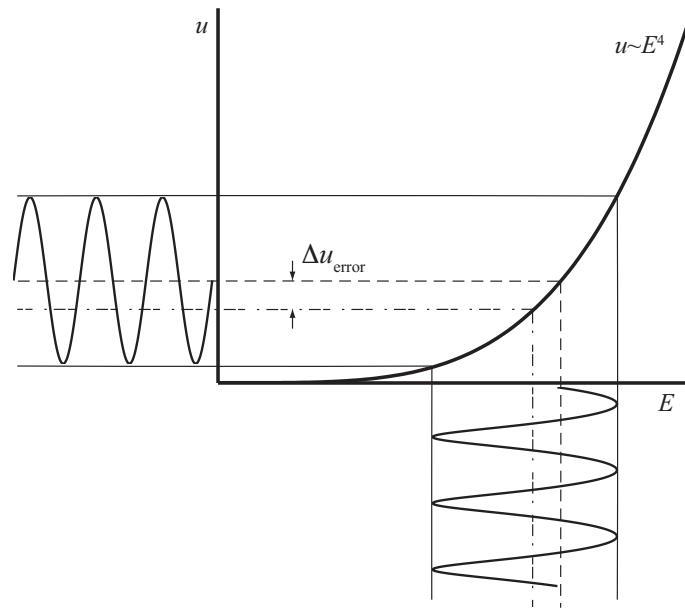
FIGURE 3.12. Illustration of the transformation of a sine from the velocity to the voltage domain. The dashed line is the mean taken in the velocity domain, whereas the dash-dotted line is the mean taken in the voltage domain.

3.4.3b. *Hot-film mass flow meters.* When thermal anemometry is used to measure mass flow rates, in industrial or technical applications, the sensor is typically applied as a metallic film on a substrate on a body which is placed inside the pipe. Such a flow meter responds to ρu so it does measure the mass flow rate. Since the output is temperature sensitive the meter usually has a temperature sensor as well in order to compensate for a change in fluid temperature. This type of flow meters can be used for high precision measurements if it is installed with care, i.e. with a sufficiently long straight pipe upstream and downstream the meter. One such flow meter is used for the reference flow rate measurement in the flow facility, used in the present study.

Hot-film mass flow meters are also commonly used in the vehicle industry to measure the mass flow rate of intake air to the engine. In that case the piping in upstream and downstream the meter is far from ideal and in that case the device needs to be calibrated for the specific geometry.

3.5. Other types of flow meters

3.5.1. *Positive displacement flow meters*

Positive displacement (PD) flow meters, directly measure the volume of fluid, flowing through the device. This is obtained by entrapping fixed volumes of the fluid in the meters inlet and dumping them to the outlet. Although some PD flow meter designs measure gas flows, liquid flow applications are the most frequent ones. Many PD configurations permit metering of the total volume of fluid passing through for a given time, which make them suitable for monitoring the consumption of water, natural gas, hydro carbon fuels etc. The device is quite accurate, and moreover, it does not require straight upstream and downstream pipe installations, for accurate estimation of flow rate. It is however not suited for pulsating flows.

3.5.2. *Electromagnetic flow meter*

The *Electromagnetic flow meter* is based on *Farraday's law of electromagnetic induction*. It can be stated as

$$E \sim Bu \tag{3.30}$$

where E is the induced electromotive force (EMF), B is the magnetic flux density and u is the velocity. This meter gives an average of the velocity over the cross section and thereby gives a volumetric measure of the flow. An advantage is that nothing is immersed into the flow so there is no extra pressure drop introduced. However, this principle does not work in non-conducting flows and is therefore only suitable for liquids, such as water.

3.5.3. *Ultrasonic flow meter*

There are a few distinct types of *Ultrasonic flow meters*. However, the principle for them is the same, namely that the ultrasound is generated in a piezoelectric transducer and is emitted in a high frequency range in the orders of tens of Megahertz. For the *Doppler flow meter* the sound wave is reflected and sensed by a receiver, and the shift in frequency of the transmitted and received waves will be proportional to the fluid velocity, by means of the *Doppler effect*. On the other hand, the *Transit time flow meter*, utilizes the fact that the time taken for an ultrasound wave traveling upstream in a flow is slightly longer than downstream. Thus, if sound waves are emitted both ways, the difference in transit time between the two waves can be related to the flow speed. In both cases, the ultrasonic meter fails to measure gas flows, mainly because of the low acoustic impedance in gases.

3.5.4. *Target flow meter*

The *target flow meter* measures the force exerted by a fluid on a bluff body suspended in the flow, using the relationship between the force and velocity,

such that

$$F = C_d A \frac{\rho u^2}{2} \tag{3.31}$$

where C_d is the drag coefficient. Target flow meters can be used in all types of fluids, but needs to be calibrated for the specific application, since it sensitive to both the density and velocity.

3.6. Summary

To summarize and get a overview of the described flow meters, they are shown in Table 1, together with characteristic properties. This table is based on data from different manufacturers of flow meters. The values should be seen as indicative.

TABLE 1. Properties of different flow measuring techniques in summary.

Measuring device	Medium	Pressure loss	Range[1]	Pipe U/D[2]	Accuracy[3]
Orifice plate	Gas/Liquid	High	3:1	20/5	±2-4% FS
Venturi	Gas/Liquid	Very low	3:1	15/5	±1% FS
Nozzle	Gas/Liquid	Medium	3:1	20/5	±1-2% FS
Laminar	Gas/Liquid	High	10:1	15/5	±1% R
Pitot	Gas/Liquid	Very low	3:1	30/5	±3-5% FS
Turbine	Gas/Liquid	Medium	10:1	15/5	±1% R
Rotameter	Gas/Liquid	Medium	10:1	None	±0.5% R
Vortex	Gas/Liquid	Medium	10:1	20/5	±1% R
Coriolis	Gas/Liquid	Low	20:1	None	±0.5% FS
Corona	Gas/Liquid	Very low	-	None	±1% FS
Thermal	Gas/Liquid	Low	10:1	20/5	±1% FS
PD	Gas/Liquid	Medium	10:1	None	±0.25% R
Electromagnetic	Liquid	None	40:1	5/3	±0.5% R
Ultrasonic	Liquid	None	10:1	20/5	±5% FS

[1] The ratio between maximum and minimum flow rates with stated accuracy.

[2] Required straight pipe section in pipe diameters: upstream (U), downstream (D).

[3] In full scale (FS) or rate (R).

CHAPTER 4

Experimental techniques and set-ups

The experiments have been carried out at the laboratory of *KTH CICERO* in a new flow rig (described also in Laurantzon *et al.* (2010*c*), Paper 1), designed to produce both stationary and pulsating flow to simulate the exhaust flow range typical for internal combustion engines for cars and medium sized trucks. In this chapter, the flow facility and its relevant hardware are described together with the installation of the various flow meters and associated measurement equipment.

4.1. Flow facility

4.1.1. *Compressors and piping system*

Pressurized air to the laboratory is provided by means of two *Ingersoll Rand* screw compressors (*Nirvana 75* and *SSR ML75*), which together deliver a maximum flow rate of 0.5 kg/s at 5 bar (gauge pressure). The compressors are coupled through a pipe system to a dryer and filter, in order to give clean and dry air to the flow rig. This part of the flow facility is placed in a rock shelter and a piping system of a length of about 30 m brings the air to the laboratory. Before entering the system flow meter, the pipe is divided into two branches just downstream an electrically controlled valve, which, together with the rest of the rig, is schematically depicted in Fig. 4.1. One of the branches is a bypass piping, which is used at low mass flow rates in order to maintain a stable flow, since the stability of the regulating valve as well as the compressors is better above a certain low mass flow rate. The other branch is the main piping to flow rigs in the laboratory. The flow rate into the test rig is measured by means of a mass flow meter of hot-film type (*ABB Thermal Mass Flowmeter FMT500-IG*). It is located downstream of a 10 m long and 100 mm in diameter, straight pipe section. Approximately two meters downstream the mass flow meter, the main pipe is in turn divided into two branches, where it is possible to chose one or the other by manual valves. One of the branches is used with an orifice plate meter to validate the calibration of the ABB thermal mass flow meter. The other pipe connects to a heater for which the power can be regulated up to 18 kW, if there is an interest or need to heat the flow going to the measurement

object. The approximate temperature increase can be estimated from

$$\Delta T = \frac{\dot{Q}}{\dot{m} c_p} \qquad (4.1)$$

which for 0.2 kg/s gives a maximum temperature increase of about 90 °C. This feature is needed when running turbines, since otherwise the temperature of the gas in the turbine may easily fall below the freezing point of the moisture in the air.
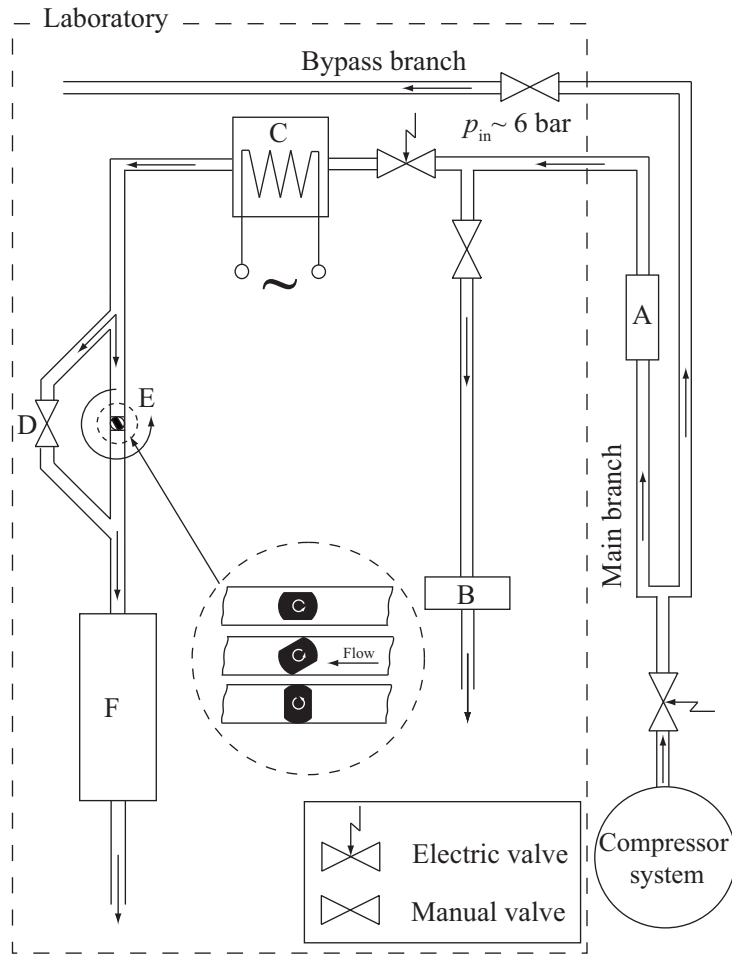

FIGURE 4.1. A schematic of the flow rig. A) Thermal mass flow meter (ABB), B) Orifice plate, C) Electric heater, D) By-pass branch, E) Pulse generator, F) Flow measurement device.

4.1.2. *Pulse generator*

A pulse generator is used to create a pulsating flow that can be used in various experiments simulating exhaust engine flows. The pulse generator consists of a rotating ball, where two symmetrically located segments has been removed. The ball is tightly fitted in the pipe system, thereby the valve opens and closes twice a revolution. The ball is rotated by an AC motor, which is operated through a frequency controlled power unit, and can be rotated with frequencies up to 50 Hz, hence giving a pulse frequency of 100 Hz. Fig. 4.2 shows the projected open valve area on a plane orthogonal to the pipe axis, as function of the angle of rotation. It is possible to add a steady flow to the pulsating flow, through a pipe branch that by-passes the pulse valve. The by-pass branch emanates $4D$ upstream the pulse valve and reconnects $4D$ downstream of it. The amount of air through the by-pass valve can be regulated by a manual valve. Downstream the rotating valve the pulse module has a pipe with a length of 320 mm, which ends immediately downstream the by-pass reconnection.
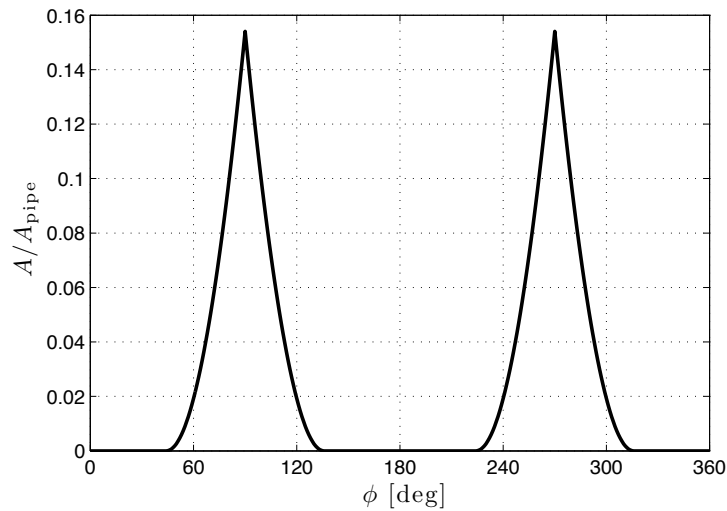

FIGURE 4.2. The projected open valve area.

4.2. Hot wire mass flow meter

In order to determine the pulsating flow coming from the pulse valve, a hot-wire mass flow meter (HWMFM) has been developed, that makes it possible to determine the instantaneous flow rate during the pulsating cycle by traversing a probe module over the cross section of the pipe. The probe module consists of a hot-wire and a cold-wire sensor in order to measure the instantaneous mass flux (ρu) and stagnation, or rather recovery, temperature. For calibration purposes of the hot-wire there are two total head probes in parallel to measure the stagnation pressure at the probe module position, whereas the spatial mean static pressure is measured through four inter-connected pressure taps at the wall.

Since the HWMFM is thoroughly described in Laurantzon *et al.* (2010*c*), Paper 2, merely some additional aspects of the meter will be mentioned in this section.

An important insight from Paper 2, is that the mass flow profile is nearly top-hat during pulsating conditions. The phenomenon that the velocity profile tends to be of plug flow character in pulsating flow, has been reported previously (see e.g. Håkansson & Delsing 1994).

4.2.1. *The hot-wire probe and calibration procedure*

The hot-wire probe itself is a welded tungsten wire with diameter $d = 5\mu$m and length $L = 1$ mm, hence giving an L/d ratio of 200. The hot-wire was operated by means of a *DISA 55M01* main frame with a *55M10* standard *constant temperature anemometry* (CTA) channel.

The hot-wire is calibrated using King's Law

$$E^2 = A + B(\rho u)^n \tag{4.2}$$

where the exponent n should be equal to 0.5 for an infinite long cylinder ($L/D \to \infty$) at 2-D steady flow, and A equal to the voltage squared at zero velocity (usually denoted by E_0) and B is a constant. Here all three constants are used in a fitting process to the calibration data and a typical calibration curve can be seen in Fig. 4.3.

4.2.2. *Temperature sensitivity*

The output from a hot-wire anemometer depends both on the mass flux and the temperature difference between the wire and the surrounding gas. If the temperature (T) of the gas during measurements differs from that of the calibration (T_{ref}), the output voltage E needs to be temperature compensated. A simple (and effective) relation for this is

$$E_{\text{comp}}^2 = E^2 \left(\frac{T_{\text{w}} - T_{\text{ref}}}{T_{\text{w}} - T} \right) \tag{4.3}$$
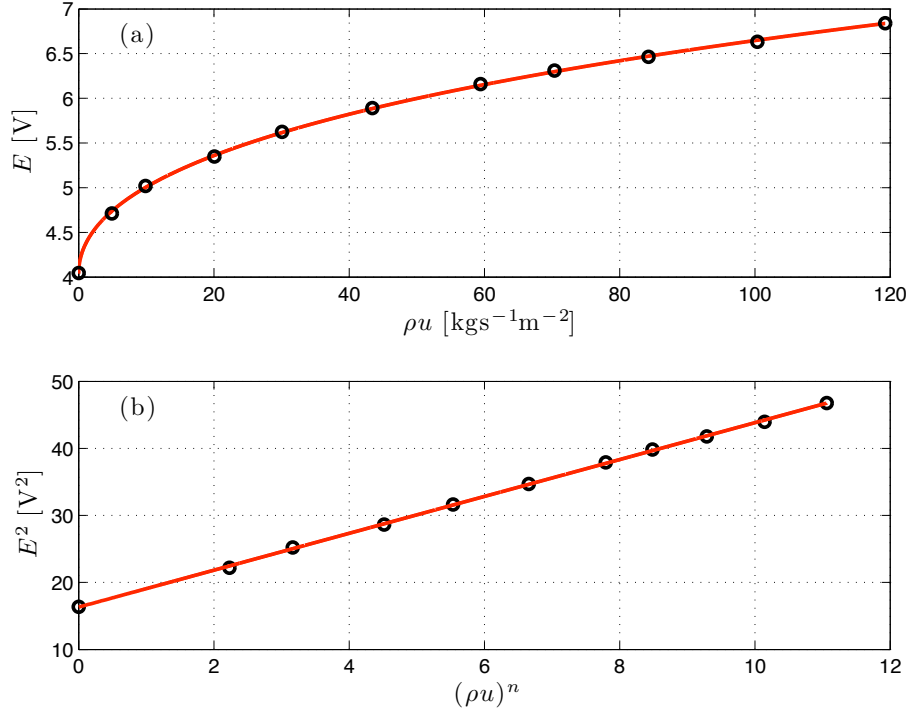
FIGURE 4.3. Hot wire calibration curve. Circles are measured calibration points, solid line is a fitted Kings law expression to the data, see Eq. (4.2). (a) E vs. ρu. b) E^2 vs. $(\rho u)^n$, for the fitted n. Here the fitting gave an exponent equal to $n = 0.50$, however n was found to vary in the range $0.42 - 0.52$ for different sensors.

where T_{w} is the wire temperature and E_{comp} the compensated voltage (see e.g. Bruun 1995, p. 215).

If the hot wire is used in a pulsating flow the stagnation temperature will change during the pulse cycle, despite the fact that the flow is adiabatic.

This means that the instantaneous hot-wire signal needs to be compensated for the changing stagnation temperature. Because the instantaneous temperature felt by the hot-wire is readily measured by means of the cold-wire exposed to the same local flow, this temperature can be directly used for the temperature compensation of the hot-wire readings.

The resistance of the hot wire is, as mentioned in the previous chapter, a function of the temperature of the hot wire according to

$$R(T_{\mathrm{w}}) = R(T_{\mathrm{ref}})[1 + \alpha_{\mathrm{ref}}(T_{\mathrm{w}} - T_{\mathrm{ref}})] \tag{4.4}$$

One parameter of importance dealing with hot-wire anemometry, is the overheat ratio of the wire

$$a_{\mathrm{w}} \equiv \frac{R_{\mathrm{w}} - R_{\mathrm{f}}}{R_{\mathrm{f}}} \tag{4.5}$$

This parameter is chosen by the user in advance. A high value of a_{w} results in high mass flux sensitivity and low temperature sensitivity, and vice versa (see Sec. 4.2.4).

If the fluid temperature varies during measurements, the output voltage signal can be compensated by combining Eqs. (4.4) and (4.5), for Eq. (4.3) to become

$$E_{\mathrm{comp}}^2 = \frac{E^2}{[1 - \alpha_{\mathrm{ref}}(T - T_{\mathrm{ref}})/a_{\mathrm{w}}]} \tag{4.6}$$

which can be used on the instantaneous hot-wire signal assuming the cold-wire is sensing the temperature relevant for the heat transfer[1]. An example with this correction employed, can be seen in Fig. 4.4. These measurement are done with the nozzle as described in Laurantzon *et al.* (2010*a*), Paper 4.

4.2.3. *Cold-wire for temperature measurements*

If the resistance wire instead is operated in *constant current anemometry* (CCA) mode it can be used for mass flux/velocity measurements, but is nowadays mainly used for the measurement of temperature fluctuations.

The CCA output was under the calibrations and measurement obtained by means of an *AN*–1003 hot-wire anemometry system (AA labs). The output from the cold-wire will in contrast to the output from the hot-wire, be a linear function of the temperature, which can be explained as follows; because the current through the wire is held constant[2], the wire voltage E_{w} will be proportional to the wire resistance R_{w}, and if we again consider Eq. (4.4), we see that $R_{\mathrm{w}} \sim T_{\mathrm{w}}$, hence it follows that

$$E_{\mathrm{w}} \sim T_{\mathrm{w}} \tag{4.7}$$

for CCA. This linear dependence can be observed in Fig. (4.5), which is a typical calibration curve for a cold-wire.

During the calibration, it is of importance to ensure that the response from the cold wire is only due to temperature fluctuations. To accomplish this, T is kept constant and u is varied, which ideally ought to give a constant cold-wire output. Furthermore, the current in CCA is set by the user; This should be sufficiently high to get good enough temperature resolution, but on the other

---

[1]It should be mentioned that the value of α, in general must be found by means of calibration, since the value provided from the supplier is for pure untreated wires, and the value can differs considerable depending on how it was mounted to the prongs (Van Dijk (1999)).

[2]A value of 0.5 mA for I was used for a wire of $d = 5\mu$m, however I can be adjusted to comply with the desired temperature resolution and velocity sensitivity.
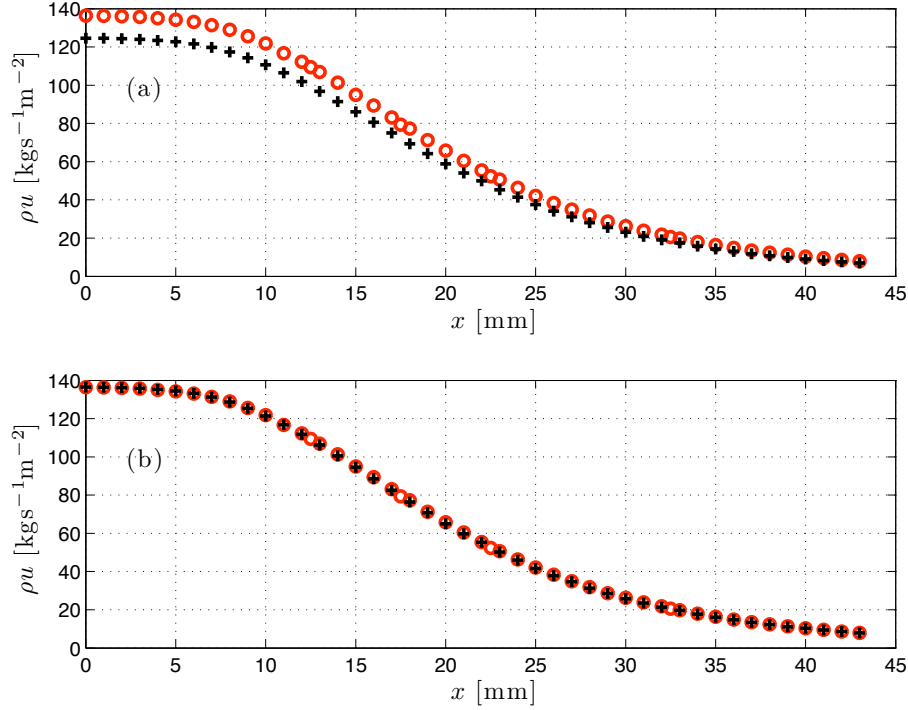
FIGURE 4.4. Mass flux measurements along a nozzle. The nozzle exit is at $x = 0$ mm and has a diameter of 10 mm. At $x = 45$ mm, the nozzle diameter is 57 mm. The calibration temperature for the hot-wire measurements were 18 °C. Measurements was made at 18 °C ($\circ$) and at 31.5 °C ($+$). (a) Output from hot-wire measurement without temperature compensation. (b) The same data, but with compensation according to Eq. (4.6), applied to the 31.5 °C measurements.

hand small enough, in order to be able to neglect velocity fluctuations (see the equations in Sec. 4.2.4, or Örlü (2006) for a more detailed discussion regarding CCA).

4.2.4. *Velocity and temperature sensitivity for CTA and CCA*

In this section a summary of velocity and temperature sensitivities are gathered for the CTA and the CCA modes as a complement to the discussion in the previous section. The results and notations in this section are mainly adopted from Bruun (1995).
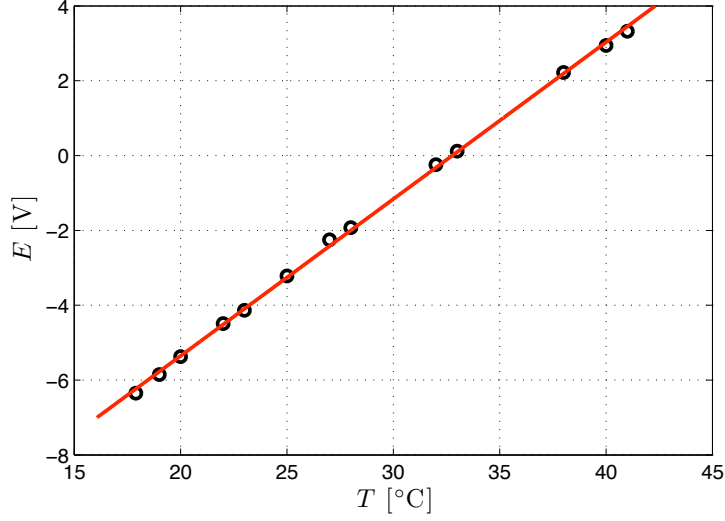
FIGURE 4.5. Cold wire calibration curve. Circles are measured points, solid line is a straight line fit to the calibration data.

The anemometer voltage E can be related to the fluctuations in mass flux and temperature, ρu and θ respectively as

$$E = S_{\rho u}\rho u + S_\theta \theta \tag{4.8}$$

where $S_{\rho u} = \partial E/\partial(\rho u)$ and $S_\theta = \partial E/\partial\theta$. The sensitivities in velocity and temperature fluctuations for the CTA and CCA mode, are:

$$S_{\rho u}^{CTA} = \frac{nB(\rho u)^{n-1}}{2}\left[\frac{R_{\mathrm{w}}(T_{\mathrm{w}} - T_{\mathrm{f}})}{A + B(\rho u)^n}\right]^{1/2} \tag{4.9}$$

$$S_\theta^{CTA} = -\frac{1}{2}\left[\frac{R_{\mathrm{w}}(A + B(\rho u)^n)}{T_{\mathrm{w}} - T_{\mathrm{f}}}\right]^{1/2} \tag{4.10}$$

$$S_{\rho u}^{CCA} = -\frac{nB(\rho u)^{n-1}I^3 R_{\mathrm{w}}^2}{R_{\mathrm{f}}(A + B(\rho u)^n)^2} \tag{4.11}$$

$$S_\theta^{CCA} = \frac{\alpha I R_{\mathrm{w}} R_{\mathrm{ref}}}{R_{\mathrm{f}}} \tag{4.12}$$

Forming the ratio of velocity to temperature sensitivity, Eqs. (4.9) and (4.10) respectively, one has

$$\frac{S_{\rho u}^{CTA}}{S_\theta^{CTA}} = -\frac{nB}{(\rho u)^{1-n}}\left[\frac{T_{\mathrm{w}} - T_{\mathrm{f}}}{A + B(\rho u)^n}\right] \tag{4.13}$$

From the above ratio we can see that, as stated before; high mass flux sensitivity is obtained when applying a high overheat ratio ($a_{\mathrm{w}} \sim T_{\mathrm{w}} - T_{\mathrm{f}}$). Moreover, a higher mass flux implies higher temperature sensitivity. Thus, at higher speeds it becomes even more important to measure the temperature accurately.

4.3. LDV measurement technique

During the measurements with various flow meters it was observed that some of the results showed a strange behavior and a suspicion arose that back flow was occurring during the pulsating cycle. In order to investigate this, *laser Doppler velocimetry* (LDV) measurements that have the possibility to also measure back flow, were performed.

The main part of the LDV measurements were made with a single velocity component *DANTEC FlowLite* system together with a BSA 60 processor. The emitting light source is a 10 mW He-Ne laser with a wave length of 632.8 nm. The emitted laser beams are converged to a measuring volume after passing a lens with focal length of 400 mm.

The seeding particles (*Shell Odina oil 27*), were injected just downstream the pulse valve through a specially constructed pipe section. An optical sensor provided a trigger signal, sensing a given valve ball angle. This signal was in turn fed to the LDV processor, thus providing means to divide the velocity measurements into phase bins during the revolution of the pulse valve.

4.4. Flow meter modules and their set-up

A number of different flow meters have been tested under stationary and pulsating conditions. All flow metering devices were mounted downstream the pulse valve module (item F in Fig. 4.1). Since the flow meters have different geometrical shapes, they have slightly different pipe connections. In all cases except one (the vortex flow meter described in Laurantzon *et al.* (2010*b*), Paper 3) a pipe was connected downstream the meter that was open to the atmosphere without any constriction. The flow meters and their installations will be described in the following text.

It should also be noted that some of the flow meters must be calibrated before use. This is the case for the hot-film flow meter, the vortex flow meter and the turbine meter. The calibration is done against the mass flow rate measured by the ABB meter. The output of the hot film meter is assumed to be directly related to ρu, i.e. the mass flux. The vortex flow meter and the turbine meter are however responding to the volume flow. In these two latter cases the density of the gas at the meter has to be estimated. An estimate is obtained by measuring the instantaneous pressure upstream and downstream the meter as well as the stagnation pressure and temperature. The flow through the meters are probably not isentropic, but this is however a reasonable approximation which is used in order to estimate the average density.

The built in processing gives the readings from the vortex flow meter and the turbine meter a steady output signal even under pulsating conditions and they are not really meant to be used under pulsating and compressible conditions. However they are included here in order to see wether they have a potential to be used to measure the mean mass flow rate under these conditions. Also the hot-film flow meters has a frequency response which limits its ability to make time resolved measurements at high pulsating frequencies.

The venturi flow meter and the Pitot tube are usually not meant for pulsating flows, however by using short response and flush mounted pressure transducers they can be used also to determine the instantaneous mass flow rate under pulsating conditions.

4.4.1. *Venturi flow meter*

The venturi flow meter used in this study is a venturi meter used in *Volvo* heavy duty trucks to measure EGR flow rate (see Fig. 4.6). In the present tests it is located approximately one meter downstream the pulse valve. The meter is connected to the pulse valve section by a straight pipe ($L = 750$ mm), with an inner diameter of 55 mm. The meter outlet is connected to a temperature measurement section and a 400 mm long pipe, leading to the ambient air. The meter has the principal design as the venturi in Fig 3.2. The device has moreover two static pressure taps, where the first tap is located at the upstream end of the meter and the second tap is located at the throat. The cross section areas at pressure tap positions are A_1=2083 mm^3 and A_2=568 mm^3, respectively. For the stationary measurements a differential pressure transducer is used, which is connected by plastic tubes to the two pressure taps. An absolute pressure transducer is also connected to the upstream pressure tap. This arrangement gives good accuracy also at low flow speed, at which the pressure difference is small. This arrangement is however not possible for the pulsating flow measurements, since the tubing-pressure transducer system has a too slow response to be able to accurately measure the pressure difference. Instead, two fast response absolute pressure transducers (*Kulite WCT-312M-25A*), were flush mounted at each pressure tap, in order to record the instantaneous variations in the pressure.

Directly downstream the venturi flow meter, a temperature measurement module with a Pt100 sensor[3] and a cold-wire is mounted. The Pt100 sensor is used during stationary measurements, but also serves as a calibration reference for the cold-wire temperature sensor used for pulsating flow. Under stationary conditions the flow is assumed to be adiabatic and the stagnation temperature T_0 is then constant both in time and along the venturi meter. However during pulsating flow the stagnation temperature will vary. The cold wire measures

---

[3]Pt100 is a resistance thermometer, commonly used as a reference sensor for temperature calibration. Pt stands for platinum and 100 is the resistance of the thermometer in ohms at 0 °C.

FIGURE 4.6. Photo of the venturi flowmeter. The flow direction is from the right to the left.

the recovery temperature T_r which has been shown to be close to the stagnation temperature T_0. If the pulsating flow can be viewed as quasi-steady then we can assume that the stagnation temperature is constant along the Venturi at each instant of time.

4.4.2. *Pitot tube*

An L-shaped Pitot tube was mounted in a short pipe module with inner diameter $D = 40$ mm, situated approximately 1.5 m downstream the pulse valve. A Pitot tube with an outer diameter of 5 mm and an inner diameter of 2.5 mm was mounted through a hole in the pipe wall. At the pipe wall/Pitot tube interface, there is a fast response pressure transducer (*Kistler 4045A5*), which is essentially flush mounted, but with a small volume in between. A short distance upstream (approximately 43 mm) the tip of the Pitot tube, a fast pressure transducer (*Kulite WCT-312M-25A*), flush mounted at the pipe wall, measures the static pressure.

The same temperature measurement module used with the venturi meter set-up, was also used in this set-up. The temperature module was mounted about 3 pipe diameters downstream the Pitot tube.

4.4.3. *Hot-film flow meter*

Two hot-film flow sensors were studied, one that was provided by *Scania*, measuring the amount of air into the engine. A second hot-film device from *Bosch*

(*HFM5*) was also evaluated. Both were run in the same set-up with a circular PVC pipe connected to the pulse module. The PVC pipe has a diameter $D = 69$ mm, and length $L = 1765$ mm, with the outlet open to the laboratory. The actual hot-film module was located about $19D$ downstream the pulse generator module, and the distance between the hot-film and the outlet was $6D$. Both hot film meters were mounted in the PVC pipe.

The modules contain a hot-film for registration of the mass flux ρu and a thermistor for temperature measurements. Both hot-film devices are commercial flow meters with a given calibration chart. However for this specific installation, they were re-calibrated in order to comply with the present geometry. The characteristic King's law behavior for stationary flow is evident for both meters, as seen in Fig. 4.7.
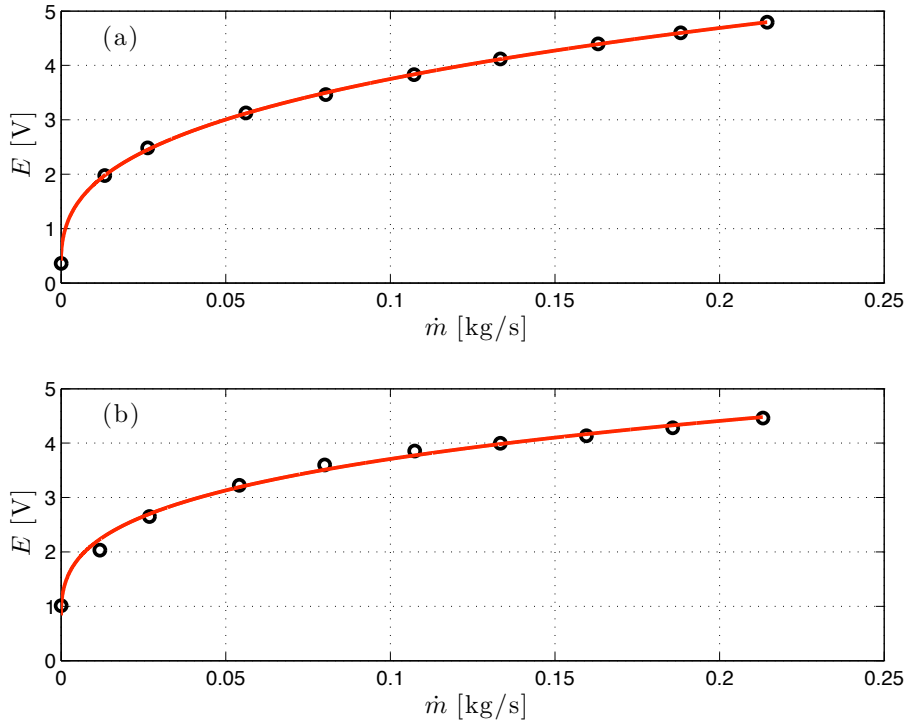
FIGURE 4.7. Hot film calibration curves for (a) Scania hot-film meter and (b) Bosch hot-film meter. Circles are measured points, solid lines are fitted data.

During the hot-film measurements a suspicion arose that back flow occurred, therefore complimentary LDV measurements were carried out under the same flow conditions but without the hot film present. To enable LDV

measurements, the PVC pipe was replaced with a Plexiglas pipe, and a glass section with a length of 200 mm was placed at hot-film meter location. The length of the combined sections was the same as the PVC pipe with the hot-film mounted. This was both to get an idea about the amplitude of the velocity fluctuations and also to determine whether back flow occurred at the position of the hot-film. This will be further discussed in the result section.

4.4.4. *Vortex flow meter*

Two types of vortex flow meters were studied, a commercial vortex flow meter and an in-house vortex flow meter, respectively, where the latter is described in detail in Laurantzon *et al.* (2010*b*), Paper 3 and is not further described here.

The commercial flow meter is a *Yokogawa DY050* vortex flow meter, where the measurement section has a diameter of 50 mm diameter and a length of 200 mm and is equipped with flanges at both ends. Furthermore, upstream the vortex flow meter a $15D$ long pipe is connected to the pulse valve module. Since the meter measures the volume flow rate, the density must be estimated in some way in order to compare it with the reference ABB flow meter. For this purpose, a fast response pressure transducer (*Kulite B57*) where flush mounted just upstream the vortex flow meter module, whereas the same pipe module used for the Pitot tube measurement, was located just downstream the meter. Finally a temperature module was placed downstream the Pitot tube pipe module. From these measurements of the pressure upstream and downstream the device as well as the stagnation pressure and temperature, an "average" fluid density at the location of the vortex meter was estimated.

To exemplify with a worst case scenario we may consider the highest flow rate which was 215 g/s. In this case the pressure drop was about 12 kPa, with an upstream pressure of 160 kPa, while the downstream end of the pipe ($5D$ downstream the flow meter) was open to the atmosphere. Assuming isentropic conditions in the flow between the pressure transducers would give a density difference of about 6% between the two tap locations. To obtain the mass flow rate, the averaged pressure and the stagnation pressure are used to determine the local Mach number. The temperature is determined from the energy equation, knowing the Mach number and the stagnation temperature. The density is thereafter obtained using the perfect gas law.

4.4.5. *Turbine flow meter*

The turbine flow meter used in the experiment is of type *GL-FL3* from *GL Flow*, which is a commercial volume flow meter

The set-up for this meter was quite analogous to that of the vortex flow meter. However, the diameter of the measurement section of the turbine flow meter is 40 mm. The difference in diameter between the upstream piping and the turbine flow meter was adjusted with a short smooth convergent pipe

section. To estimate the mass flow rate an average density of the gas was estimated in a similar way as for the vortex flow meter. However in this case the pressure difference across the meter is much larger, at 215 g/s the pressure upstream the meter was 191 kPa and the pressure drop 41 kPa. Of course, this increases the uncertainty in the determination of the density.

During pulsating conditions the output from the turbine flow meter was constant, and the variable mass flow rate under pulsating conditions was determined from the density variations obtained from the pressure and temperature measurements.

CHAPTER 5

Results

In this chapter we describe the measurements carried out with a number of different flow meters, both under steady and pulsating flow. The flow facility Thermal Mass Flow Meter from ABB has served as a reference mass flow measuring device. Some of the flow meters need to be calibrated before use. This is done under steady conditions with the use of the ABB flow meter thereby establishing a relation between the flow meter output and the real flow rate. This relation is then assumed to be valid and is employed under pulsating flow conditions.

5.1. Hot wire mass flow meter

The purpose of the hot-wire mass flow meter (HWMFM) is mainly to serve as a reference for flow measurement, especially at pulsating conditions, when it accurately can do time resolved flow measurements by automatically traversing the cross section of the pipe downstream of the pulse generator. For details of the measurement procedure, the reader is referred to Laurantzon *et al.* (2010*c*), Paper 2. The results shown in that paper were obtained with a turbine downstream of the HWMFM whereas the results shown here are with the gas flowing directly out into the laboratory, which is also the case for the results of the different flow meters that are analyzed.

The measurements were done at two nominal[1] mass flow rates 80 g/s and 130 g/s respectively, as measured by the ABB flow meter and at three different pulse frequencies, i.e. 40, 60 and 80 Hz. Unfortunately it was found that the measurements at 80 g/s at 80 Hz were corrupt, probably due to a damaged hot wire, so only five cases are available.

To obtain the time resolved mass flow rate each measurement position of the hot-wire is phase averaged, and thereafter the flow rate is obtained through an integration over the pipe cross section. As described in Paper 2 the hot wire is traversed both radially (7 positions, including the centerline) and azimuthally (12 angles, 30° apart) to in total 84 points evenly distributed in the pipe cross section. The phase averaged quantity, will to a high degree resemble a low pass filtering of the time signal, since the turbulence time scales are much shorter than the pulse period.

---

[1] The deviation from the given values are for all measurements less than 3 %.

Figs. 5.1 and 5.2 show the measurements for the flow rates 80 and 130 g/s, respectively. In each figure both the 40 and 60 Hz pulse frequencies are shown. In the upper subfigures an example of the instantaneous mass flux signal obtained at the centerline is shown together with the phase averaged signal. In the lower two subfigures the integrated mass flow rate for the two pulse frequencies are shown. The average mass flow rate obtained from the ABB reference meter is also shown through a dashed horizontal line. One may note that the turbulent fluctuations shown in the instantaneous signal is of an order of magnitude lower amplitude than the amplitude of the pulses themselves.

In Table 1 the measured flow rates obtained with the HWMFM are shown both for steady and pulsating flows. All measured flow rates are normalized with the flow rate obtained from the ABB flow meter. As can be seen the measured flow rates are within $\pm$ 3% of the reference value. This despite the fact the there may be a short period of back flow during the pulsation cycle as indicated in Sec. 5.1.1.[2]

$\dot{m}$	Normalized flow rate			
	$f_p = 0$ Hz	$f_p = 40$ Hz	$f_p = 60$ Hz	$f_p = 80$ Hz
80 g/s	1.01	0.997	1.01	-
130 g/s	0.968	0.979	0.988	1.02

TABLE 1. Mass flow rate obtained from the HWMFM (normalized with the reference mass flow rate).

The phase averaged mass flux profiles are plotted for five different phases in Fig. 5.3 at 80 g/s mean mass flow rate. This can also be seen in Laurantzon *et al.* (2010c), Paper 2. The difference however is that in the present case the air is flowing to the ambient atmosphere downstream the HWMFM, whereas in the other case, the HWMFM was connected to a turbocharger. This difference gives somewhat different pulse appearance with respect to the fluctuations, albeit more or less unchanged mass flux profile.

---

[2]The measurements performed under pulsating conditions, were not compensated for temperature variations.
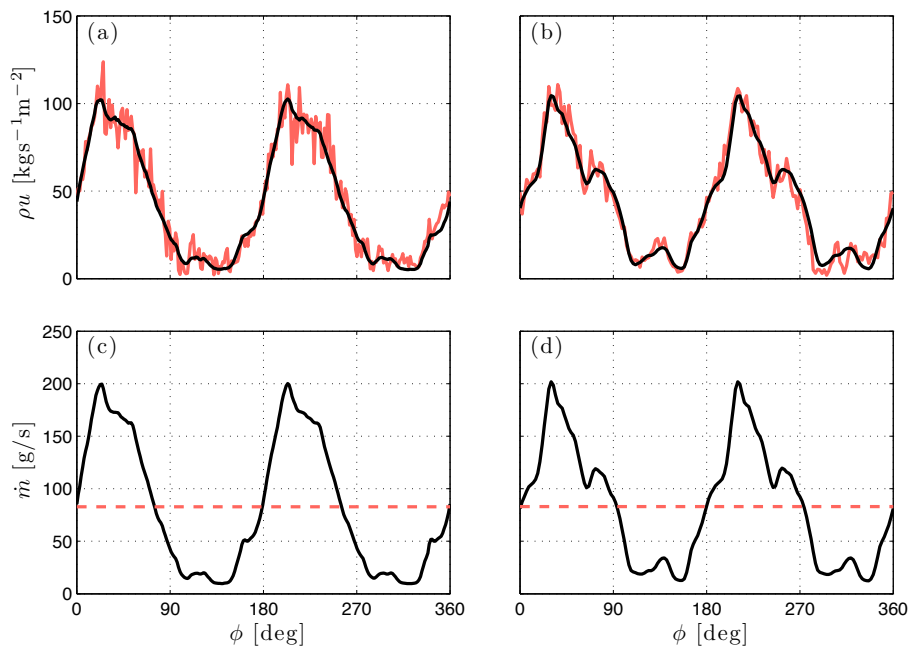
FIGURE 5.1. Results from the hot wire mass flow meter at a flow rate of 80 g/s. (a) and (b) instantaneous mass flux (ρu) measured on the pipe centerline, together with the phase averaged signal (solid black line) for pulse frequency of 40 and 60 Hz, respectively. (c) and (d) phase averaged mass flow rate for pulse frequency of 40 and 60 Hz respectively. The horizontal dashed line represents the mean mass flow rate.
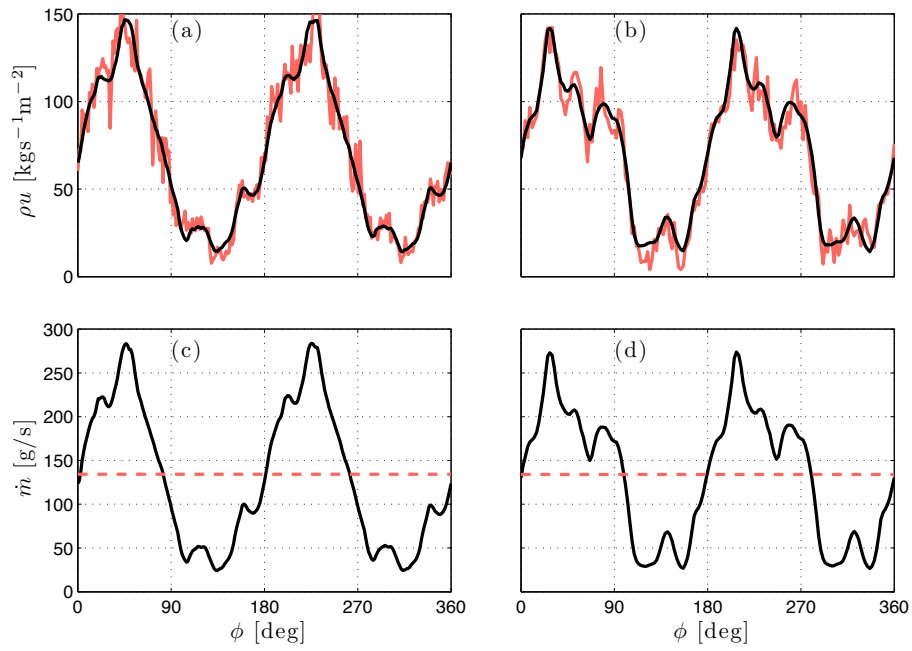
FIGURE 5.2. Results from the hot wire mass flow meter at a flow rate of 130 g/s. (a) and (b) instantaneous mass flux (ρu) measured on the pipe centerline, together with the phase averaged signal (solid black line) for pulse frequency of 40 and 60 Hz, respectively. (c) and (d) phase averaged mass flow rate for pulse frequency of 40 and 60 Hz respectively. The horizontal dashed line represents the mean mass flow rate.
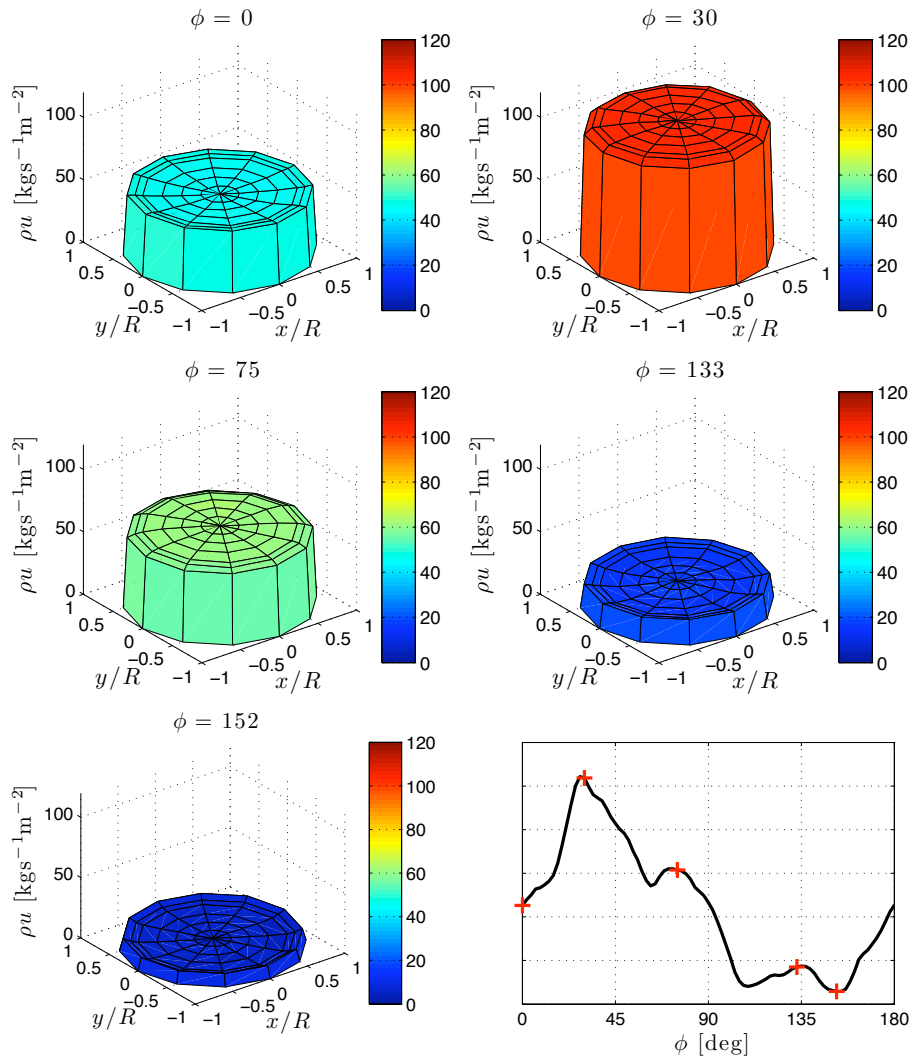
FIGURE 5.3. Mass flux profile in the pipe cross section for five different phases. The lowest right plot is the mass flux measured on the centerline and phased averaged. The five locations for the profiles are marked with +.

5.1.1. *Laser Doppler Velocimetry*

For a separate check on the flow conditions measurements were performed using the LDV system described in Sec. 4.3. The measurements were performed about 30 cm downstream of the hot-wire position when using the HWMFM. The HWMFM was replaced with a dummy section with the same geometry as the HWMFM. The dummy section (as is the HWMFM) is converging after the test section and changes from a diameter of 50 mm to 40 mm. The LDV measurements are carried out at the outlet of the dummy section so the velocity here (assuming constant density and a plug flow profile) should be approximately 1.56 times that of the section where the hot wire measurements are made.

In Fig. 5.4 the phase-averaged velocities at 80 and 130 g/s, with pulse frequencies of 40 and 60 Hz are shown. The maximum velocities shown increases with the mass flow rate as expected, but also with the pulse frequency. To be able to compare with the mass flux obtained by the HWMFM at the centre line, these velocities should be divided by 1.56 and the multiplied by the density at the outlet, which should be close to 1.20. For instance at 130 g/s and 40 Hz the maximum velocity is about 180 m/s, which would be equivalent to a mass flux of 140 kg/s which is close to what is observed in Fig. 5.2.

From Fig. 5.4 it is clear that for the 60 Hz pulse frequency both mass flow rates show a small back flow component during a short period of the phase. With the knowledge of back flow that region can also be identified in figures 5.1(d) and 5.2(d), however the phase where back flow occurs does not overlap between the two measurements since the LDV measurements are carried out further downstream as compared to the HWMFM. For the 40 Hz pulsations no back flow is observed, although the instantaneous velocity comes very close to zero.
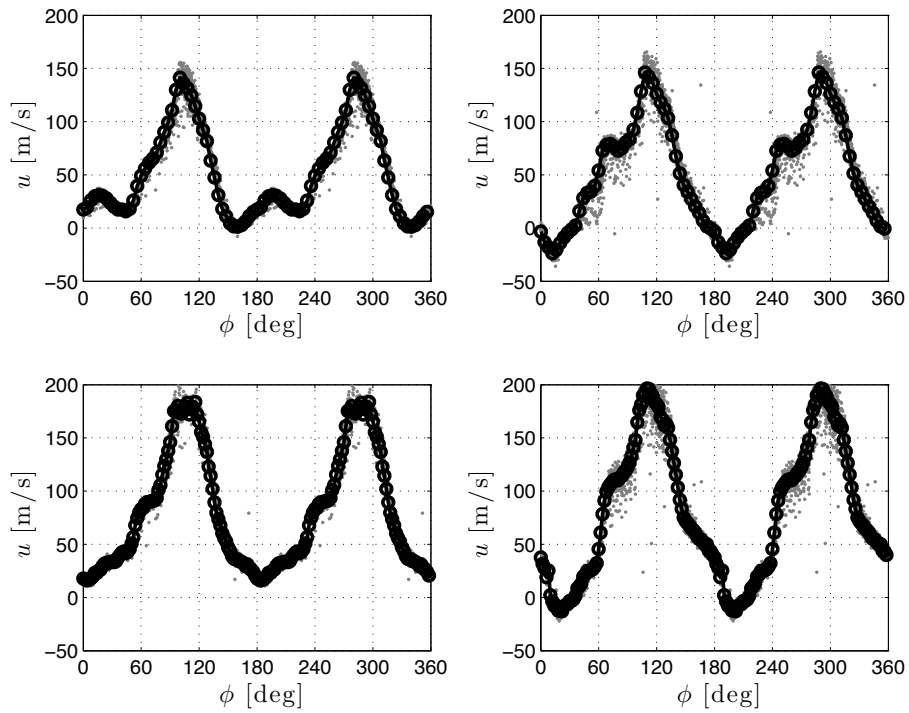
FIGURE 5.4. Measurements at the centerline using LDV. All data points acquired per phase (grey dots) and the phase averaged velocities (black circles) at 40 and 60 Hz pulse frequency, left and right respectively, at mass flow rates 80 g/s and 130 g/s, upper and lower respectively.

5.2. Venturi flow meter

Here we present flow meter measurements done with the venturi flow meter obtained from Volvo for both stationary and pulsating flow. As described in Sec. 4.4.1 the steady flow measurements were made using a differential pressure transducer between the pressure tap at the upstream wide section and the section having the smallest cross section area. For the pulsating flow two absolute pressure transducers were used to measure the upstream and downstream pressures.

5.2.1. *Stationary flow*

For stationary flow through constriction flow meters such as the venturi flow meter the estimation of the mass flow rate can be done in several ways. One way is to assume incompressible and isentropic flow and to do corrections for the compressibility as described in Chap. 3.

However in many applications this will not give reliable results and here we will analyze the flow meter using the compressible flow equations described in Chap. 2.

First we should mention that the venturi flow meter can be run in two different regimes, i.e. non-choked and choked conditions respectively. Under choked conditions the Mach number reaches unity at some position along the venturi (at the smallest section from a fluid dynamic point of view). The behavior in the two regimes are quite different as will be shown below. For the venturi the outlet in the present set-up is connected directly to the atmosphere. This makes the outlet pressure equal to the atmospheric pressure, whereas the flow rate is changed by changing the inlet pressure.

From the measured data it is possible to calculate the mass flow rate through the venturi from the isentropic relations. The mass flow rate was defined by Eq. (2.8) and it can be rewritten in terms of pressure, Mach Number and total temperature to become

$$\dot{m} = \frac{p_1 A_1 M_1}{\sqrt{RT_0}} \sqrt{\gamma \left(1 + \frac{\gamma - 1}{2} M_1^2 \right)} \tag{5.1}$$

The Mach number at the upstream cross section M_1 can be obtained from Eq. (2.30) since the pressures p_1 and p_2 are measured and the area ratio A_1/A_2 is known.

In order to illustrate the behavior of the venturi meter 10 mass flow rates ranging from 0 g/s to slightly above 200 g/s were used for the stationary measurement. This flow range includes both non-choked (7 measured points including zero flow rate) and choked conditions (3 measured points).
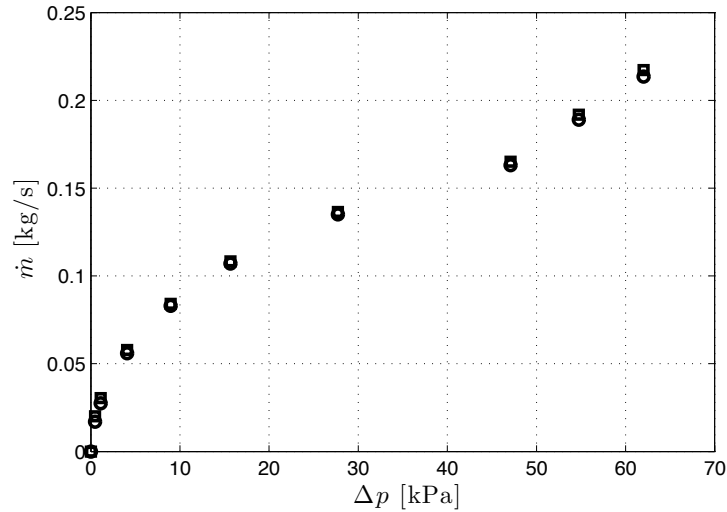
FIGURE 5.5. Mass flow rate for the venturi flowmeter at stationary flow as function of the pressure difference $\Delta p = p_2 - p_1$. □: Calculated flow rates from measured flow data and venturi geometric data. ○: Mass flow rate according to the ABB reference flow meter.

The measured mass flow rate is plotted as function of the pressure difference $\Delta p = p_1 - p_2$ in Fig. 5.5, where p_1 is measured upstream the venturi contraction and p_2 is measured in the middle of the (geometrically) smallest section. Together with the measured data the calculated mass flow rates from Eq. (5.1) are also plotted in the figure. As can be seen there exist two different regimes, one up to a pressure difference of about 40 kPa and another above that value. In the first regime the mass flow rate increases almost parabolically with the pressure difference, which is what is expected for incompressible flow. In the upper regime there is a linear trend with increasing pressure. For choked flow we would expect the flow rate to increase linearly with the stagnation pressure which is reflected as the linear trend in the Fig. 5.5. The agreement between the calculated values and the measured flow rates are overall good, however at small pressure differences there are some discrepancies which probably is due to uncertainties in the measured pressure difference. At high pressure ratios (in the choked regime) the calculated values are higher than the measured (1.2-1.7 %).

In Fig. 5.6 the same data as in Fig. 5.5 are instead plotted as function of the pressure ratio p_2/p_1, also here together with the theoretically obtained results (based on the measured area and pressure ratios). The choked flow regime is now clearly seen around a pressure ratio of 0.62. From the isentropic
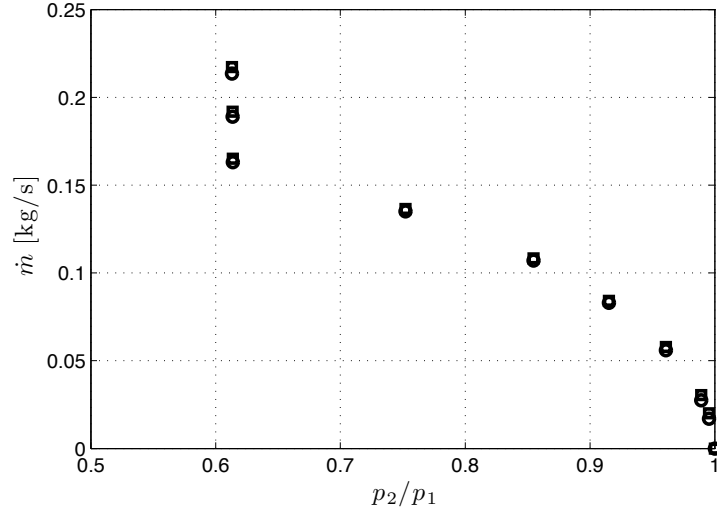
FIGURE 5.6. Same data as in figure 5.5, however here the data are plotted as function of the pressure ratio p_2/p_1. □: Venturi flow meter, ○: ABB reference flow meter

relationships we know that at critical conditions the pressure ratio $p^*/p_0 = 0.528$. Here $p_1 \neq p_0$ but should be about 1.5% smaller (based on $M_1 = 0.15$), which hence does not explain this difference. So the obvious conclusion is that the measured pressure at the throat is not at the smallest, in a fluid dynamic sense, section. Thus, the conditions at the second pressure tap is not the critical condition, but a Mach number less than unity, and the flow is further accelerated in the straight part of the nozzle until it reaches the critical condition.

As the upstream pressure is increased the flow rate increases, and the Mach number at the venturi throat will reach unity, for high enough difference pressure (or rather pressure ratio). As shown in Chap. 2, the mass flow rate then becomes a linear function of the stagnation pressure. This feature is apparent for the three last points in Fig. 5.5, where one can see the linear dependence between mass flow rate $\dot{m}$ and the difference pressure Δp.[3] The expression for the mass flow rate at choked nozzle flow (repeated here again for convenience) is

$$\dot{m} = \frac{p_0 A^*}{\sqrt{RT_0}} \sqrt{\gamma \left(\frac{2}{\gamma + 1} \right)^{(\gamma+1)/(\gamma-1)}} \tag{5.2}$$

---

[3] Δp is in fact linearly proportional to p_0 at choked conditions.

If instead we write it as function of p^*, the above relation can be rewritten to obtain

$$\dot{m} = \frac{p^* A^*}{\sqrt{RT_0}} \sqrt{\frac{\gamma(\gamma+1)}{2}} \tag{5.3}$$

Consider again Fig. 5.5, we find that the mass flow rate obtained with the venturi deviates from the reference flow meter with a maximum of about 2%, and hence the theory gives a fairly good estimate of the flow rate. For the three largest flow rates however, when the flow is choked, the Mach number M_1, based on the pressure and area ratios p_2/p_1 and A_1/A_2 respectively is calculated to 0.156. In turn, this Mach number implies that $M_2 = 0.882$. Furthermore, the measured pressure ratio p_2/p_1 at choked flow is 0.614, whereas it becomes 0.537 if the isentropic relation Eq. (2.29) is employed. This result together with the fact that the pressure is measured at the middle of the throat section, suggests that the flow becomes sonic further downstream at the end of the throat section.

In order to test this hypothesis we do the following analysis. The throat section of the venturi is not distinct, but has some distance of "more or less" constant cross section. Assume that the flow in the throat section, from the second pressure hole to the end of the throat, where we assume that the Mach number is unity (denoted location 3), develops according to adiabatic one-dimensional flow theory with friction (so called Fanno-flow, see Sec. 2.2.4). This distance is of course short and is of the order of the throat diameter. Consider Eq. (2.24), if $L \simeq D$ then the ratio $4fL/D$ becomes 0.02, assuming $f = 0.005$. This corresponds to a Mach number of about 0.88, which is close to what we estimated at section 2 from the measured pressure ratio.

Furthermore, regarding the pressure ratio, consider Eq. (2.23). It is possible to obtain a general expression for the pressure ratio between the pressure at Mach number M and the pressure at critical condition by substituting $M_2 = 1$ and M_1 to just an arbitrary Mach number M, with the corresponding pressures p^* and p respectively, to become

$$\frac{p}{p^*} = \frac{1}{M} \sqrt{\frac{\gamma+1}{2 + (\gamma-1)M^2}} \tag{5.4}$$

This relation is plotted in Fig. 5.7. Considering the plot, one can see that when the Mach number is 0.88 the pressure ratio $p/p^* = p_2/p_3$ is about 1.16 (this can of course also be obtained directly from Eq. (5.4). With the previous measured and estimated values we have that $p_2/p_1 = 0.614$ and $p_3/p_1 = 0.537$ and hence, $p_2/p_3 = 0.614/0.537 = 1.14$, showing a good agreement with the theoretical pressure ratio.
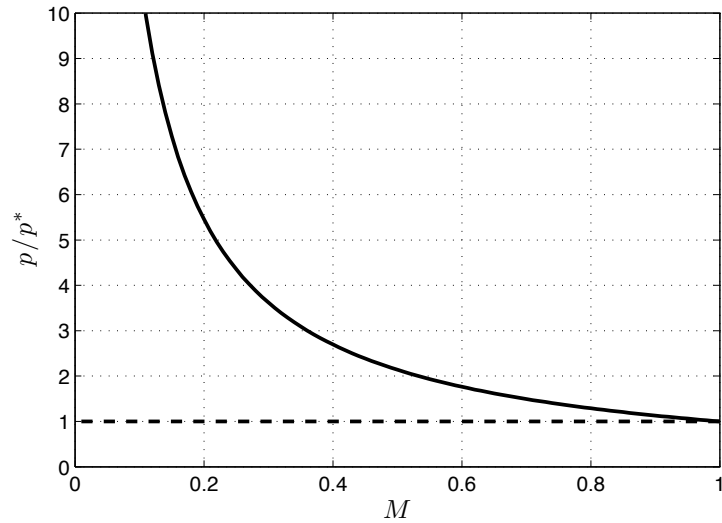
FIGURE 5.7. Pressure ratio between the pressure at Mach number M and the pressure at critical condition, assuming one-dimensional adiabatic flow.

5.2.2. *Pulsating flow*

The response of the venturi flow meter to pulsating flow was investigated at two mass flow rates, i.e. 80 g/s and 130 g/s. For 80 g/s the frequency of the pulsating flow ranges from 10 Hz up to 80 Hz in 10 Hz steps, whereas for 130 g/s, measurements were made at pulse frequencies of 40, 60 and 80 Hz. As mentioned before, but repeated here, for the pulsating flow cases the pressures p_1 and p_2 were measured directly with an absolute pressure transducer mounted directly on the pressure tap.

The estimation of the mean mass flow rate under the pulsating conditions can be done in two ways. One possibility is to calculate the mean pressures of p_1 and p_2 and thereafter determine a mean Mach number M_1 from Eq. (2.30). This will however, as we shall se, lead to drastic overestimation of the flow rate. The other possibility is to assume that the flow is quasi-steady, and to employ Eq. (2.30) at each time instant to calculate the instantaneous value of M_1. In this way, the time resolved mass flow rate can be obtained from Eq. (5.1), and then the mean of this time varying quantity can be determined. These two method are compared in Table 2, where the average mass flow rate is about 80 g/s for each pulse frequency.

Method	10 Hz	20 Hz	30 Hz	40 Hz	50 Hz	60 Hz	70 Hz	80 Hz
Mean	1.365	1.387	1.500	1.395	1.210	1.108	1.177	1.073
Inst.	1.023	1.062	1.092	1.052	1.001	1.013	1.007	1.016

TABLE 2. Mass flow rate estimation (normalized with the reference mass flow rate of 80 g/s) for the two methods, where "Mean" denotes the method where the flow rate is determined from the mean values of the pressures, whereas for "Inst." the time resolved mass flow rate is used to determine the mean mass flow rate.

From the results in Table 2, one can conclude that it is preferable to obtain the mean mass flow rate after the instantaneous mass flow rates are calculated. The highest deviation from the reference flow meter is about 9 %, for this method, whereas it deviated as much as 50 % for the mean case. Similar results were obtained for the 130 g/s case shown in Table 3.

Method	40 Hz	60 Hz	80 Hz
Mean	1.129	1.087	1.116
Inst.	1.034	1.020	1.049

TABLE 3. Mass flow rate estimation (normalized with the reference mass flow rate of 130 g/s) for the two methods, where "Mean" denotes the method where the flow rate is determined from the mean values of the pressures, whereas for "Inst." the time resolved mass flow rate is used to determine the mean mass flow rate.

To fully appreciate how the pressures p_1 and p_2, the stagnation temperature T_0, the pressure ratio p_2/p_1, mass flow rate $\dot{m}$ as well as the Mach numbers M_1 and M_2, varies under the pulsations, these quantities were phase-averaged. Two cases are shown in Figs. 5.8 and 5.9.[4] It should again be emphasized, that the pressures and the (stagnation) temperature are measured, whereas the mass flow rate and Mach numbers are calculated based on these measurements.

In Fig. 5.8 we see that during part of the pulse cycle the pressures p_1 and p_2 are almost identical which means that the flow rate is close to zero. One can also see that there is a plateau in the Mach numbers M_1 and M_2 that indicates that the flow is choked. According to the stationary case (see Fig. 5.6), choking occurs approximately at a mass flow rate $\dot{m} \approx 0.15$ kg/s

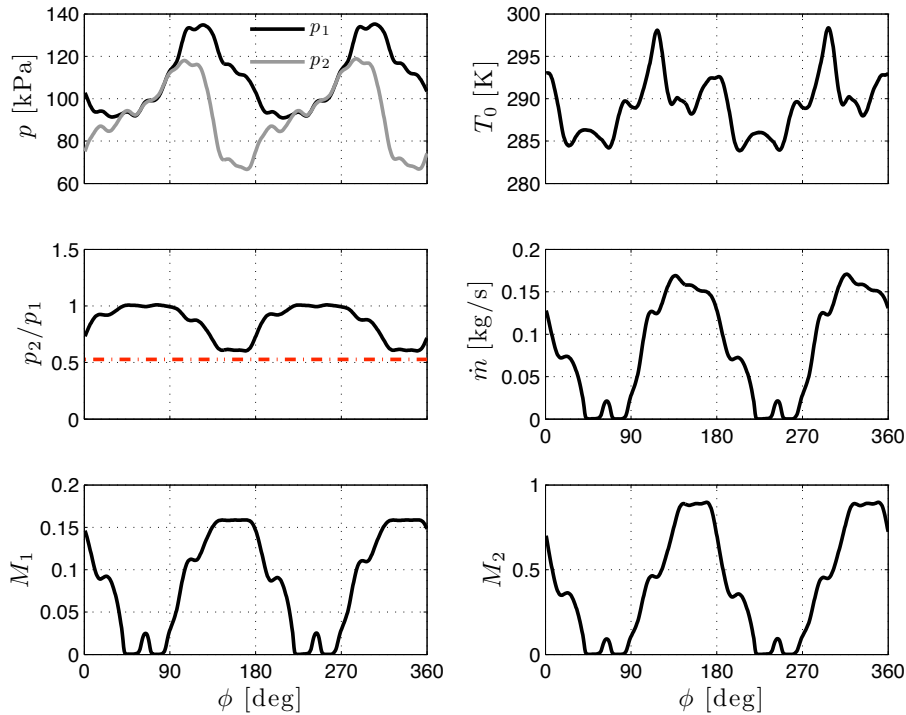---

[4]Four other cases are shown in Appendix A.

FIGURE 5.8. Venturi flow meter phase averaged data at 80
g/s and 40 Hz pulse frequency.

which seems to be the case also here. Hence the assumption of quasi steady
flow seems to be appropriate. Also for this case we observe that M_2 at choking
is less than unity, again implying that critical conditions are reached further
downstream. Finally the temperature variation during the pulsation is about
13 K. The lowest temperatures are seen at low flow rates.

Fig. 5.9 shows the same flow rate as above but with twice the pulse fre-
quency. Here we observe that the variation in pressure between p_1 and p_2 is
much smaller and the flow does not reach choking conditions. An interesting
aspect is that the number of pulsations recorded in the mass flow rate is twice
that of the pulse frequency. The reason for this is not clear, but is probably
due to pulse reflections in the system and needs to be analyzed further. As
shown in Table 2 the method using the instantaneous values of the pressures
to calculate the flow rate gave an error of only 1.6%, but also using the method
to first calculate the average pressures and then calculating the mass flow rate
showed an error of 7.3% which was the lowest of the cases reported.
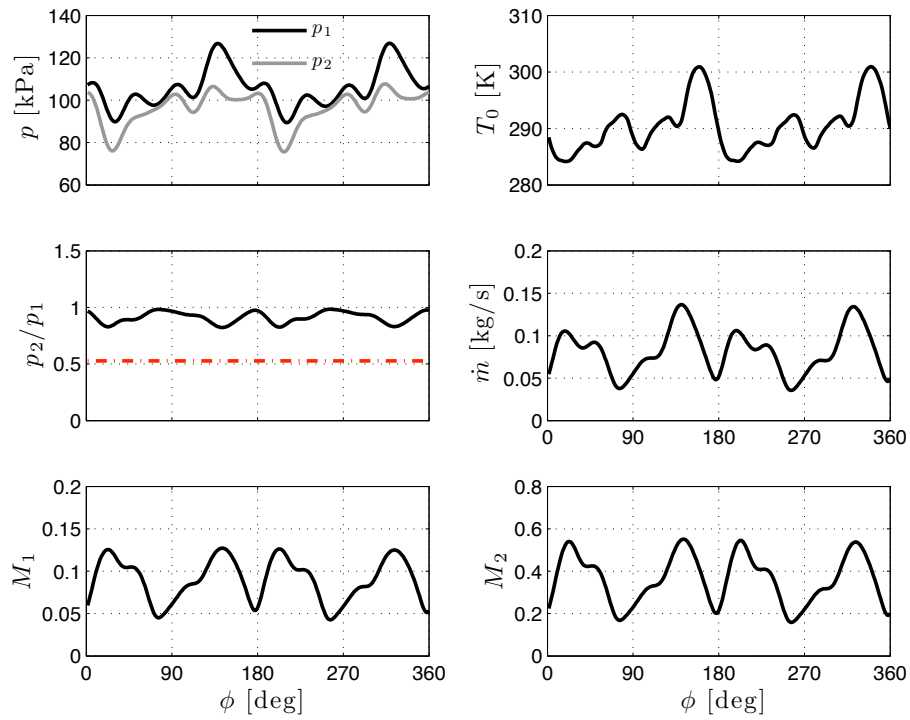
FIGURE 5.9. Venturi flow meter phase averaged data at 80 g/s and 80 Hz pulse frequency.

5.3. Pitot tube

A possibility to measure the flow rate in both stationary and pulsating (under the assumption of quasi steadiness) flow is to use a Pitot tube immersed in the flow to determine the stagnation pressure (p_0) combined with measurement of the static pressure (p) at the wall. From these values the Mach number at the position of the probe can be determined. The mass flow rate is determined from

$$\dot{m} = C\frac{pAM}{\sqrt{RT_0}}\sqrt{\gamma\left(1 + \frac{\gamma - 1}{2}M^2\right)} \tag{5.5}$$

where the Mach number is determined from the pressure ratio p_0/p according to Eq. (2.19). A is here the pipe cross section area at the position of the Pitot tube. The stagnation temperature T_0 also needs to be measured. C is a parameter that takes into account that the velocity measured by the Pitot tube is not the average velocity across the pipe section (which may depend on the flow rate). In order to take this into account the set-up can be calibrated against the system mass-flow meter to determine C under steady conditions. However, under pulsating conditions one has to assume that the ratio between the instantaneous Mach number obtained from the Pitot tube and the cross section averaged Mach number is the same.

In order to find the mass flow rate under pulsating conditions it is necessary to be able to make time resolved measurements of both the static pressure as well as the stagnation pressure. To do so in the present experiments the pressure transducers were mounted directly on the probe tubing for the Pitot tube and directly at the wall tap for the static pressure measurements. It was noted that the signal from the Pitot tube showed a high frequency component at a certain, more or less, fixed frequency for different flow rates and pulse frequencies. This implies that it is not coupled to the flow, but to something else. This phenomenon only occurred for the transducer connected to the Pitot tube. Thus, a hypothesis was that the Pitot tube connection between the transducer and the tube functioned as a *Helmholtz resonator*[5]. The resonance in a pressure transmitting tube-cavity combination is a well known phenomenon (cf. Sieverding *et al.* 2000). The Helmholtz eigenfrequency is given by

$$f_r = \frac{a}{2\pi}\sqrt{\frac{A_t}{LV}} \tag{5.6}$$

where a is the speed of sound, A_t is the throat cross section area, L is the length of the throat and finally, V is the volume of the cavity.

In order to investigate if the Pitot tube system acts as a Helmholtz resonator, a qualitative analysis of the response from the pressure transducer was

---

[5]This phenomenon occurs for flows at cavities and give rise to air resonance. It is the acoustic counterpart to the mechanic mass-spring system.

performed. For this analysis, measurements at stationary conditions were performed when the pressure transducer was screwed in the bottom of its thread. The distance between the face of the pressure transducer and the Pitot tube give rise to a cylindrical cavity volume with an estimated height of 0.5 mm and with the diameter of the pressure transducer, which is 13 mm. Together with the length of the Pitot tube $L = 44$ mm and the cross section diameter of the Pitot tube $D_t = 1.8$ mm, the resonance frequency can be determined from Eq. (5.6) to about 1.6 kHz. A spectrum obtained from the time signal of the pressure transducer connected to the Pitot tube can be seen in the top plot of Fig. 5.10, where most of the energy is concentrated to about 1.55 kHz. The two lower plots are obtained when the pressure transducer was screwed out in two steps, i.e. the cavity volume was increased in two steps. This would, according to Eq. (5.6), imply a lower resonance frequency, which also can be observed from the spectra. Hence the hypothesis that the high frequency content of the Pitot tube signal is due to a Helmholz resonance seems to be confirmed.
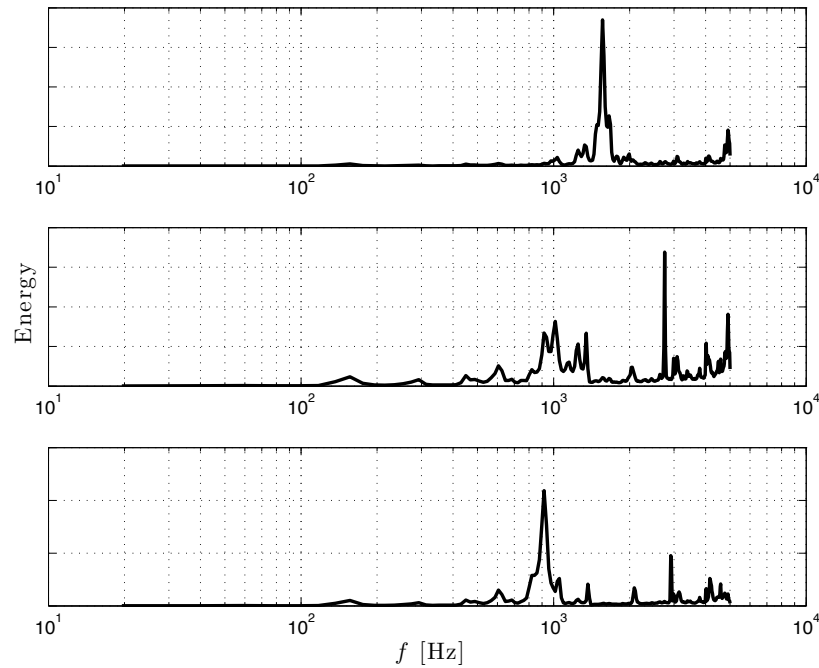
FIGURE 5.10. Pre-multiplied spectrum from three cases of chamber size, to test the hypothesis of a Helmholtz resonator. The chamber volume increases from the top to the bottom plot.

5.3.1. *Stationary flow*

The stationary measurements, were mainly done in order to calibrate the mass flow rate obtained from the Pitot tube against the reference mass flow meter. Since the Pitot tube just measures the total pressure at the centerline, and the *bulk velocity*[6] is in general lower than the centerline velocity for pipe flow, the mass flow estimated with the Pitot tube will overestimate the flow rate. Hence, this ratio has to be determined by means of the calibration. The relation between the reference mass flow determined by the system mass flow meter and that obtained by the Pitot tube assuming that it senses the bulk flow rate. As is shown in Fig. 5.11, this gives that the mass flow rate obtained from the Pitot tube measurements overestimates the actual flow rate with approximately 13%. The linear dependence between the two methods indicates that the parameter C in Eq. (5.5) is independent of flow rate in the stationary case.
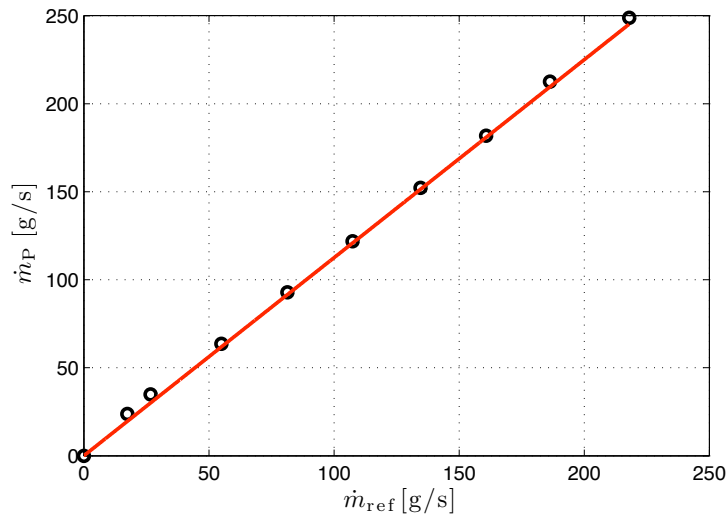
FIGURE 5.11. The mass flow rate obtained with the Pitot tube vs. the reference ABB flow meter. The solid line is a linear fit.

5.3.2. *Pulsating flow*

The pulsating flow measurements were performed at the same flow rates and pulse frequencies as for the venturi flow meter. The stagnation and static pressures p_0 and p were both sampled at 10 kHz, but had to be low-pass filtered afterwards due to the high frequency noise content in the signal due to the

---

[6]This is the velocity one obtains if the mass flow is divided by ρA, i.e. in some sense, the average velocity over the cross section.
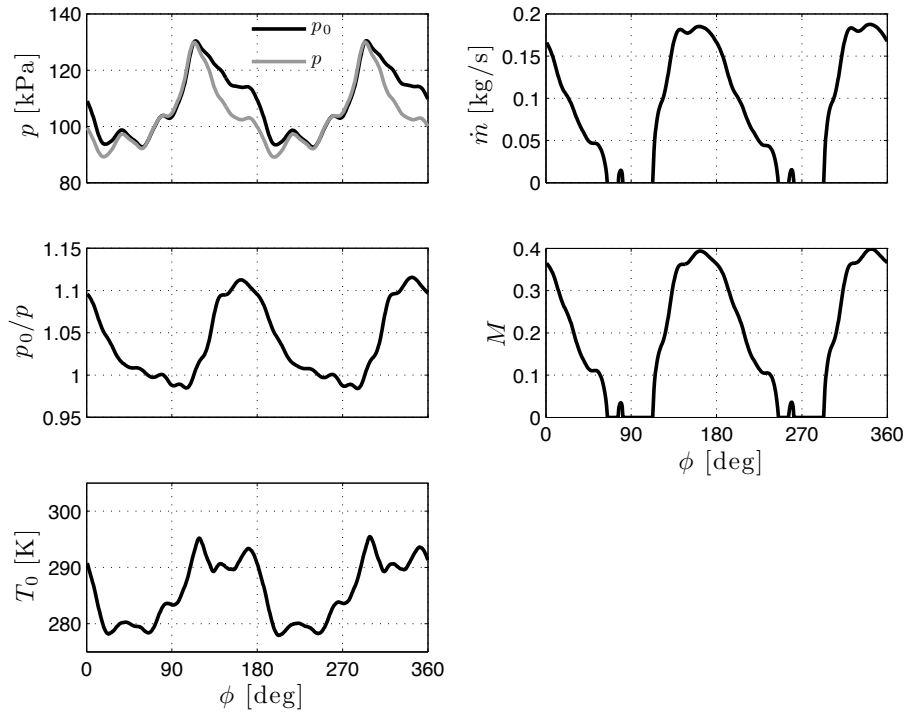
FIGURE 5.12. Pitot tube measured phase averaged quantities
at 80 g/s flow rate and 40 Hz pulse frequency.

Helmholtz resonance. To obtain the flow rate the pressure signals are first sampled and phase averaged individually and the pressure ratio p_0/p was calculated from the phase averaged signals. From the pressure ratio the Mach number is calculated and together with the static pressure and stagnation temperature the mass flow rate is calculated using Eq. (5.5). assuming that the ratio between the mass flow rate and that measured by the Pitot tube i.e. parameter C is the same in the stationary and the pulsating flow. It was observed that for short periods, when the flow was rapidly accelerating, the recorded pressure ratio was less than unity, which of course is physically not possible, but can be due to a time lag in the Pitot tube measurements. For these periods the pressure ration was set to zero, i.e. the Mach number and hence the flow rate were both set to zero.

In Figs. 5.12 and 5.13, the measured quantities p_0, p as well as the pressure ratio p_0/p and the measured stagnation temperature T_0 are plotted together with the calculated M and $\dot{m}$. For the 40 Hz pulsation case one peak in pressure and mass flow can be seen for each pulse from the pulse generator. In this case one can see that the pressure ratio becomes less than one for a short period,
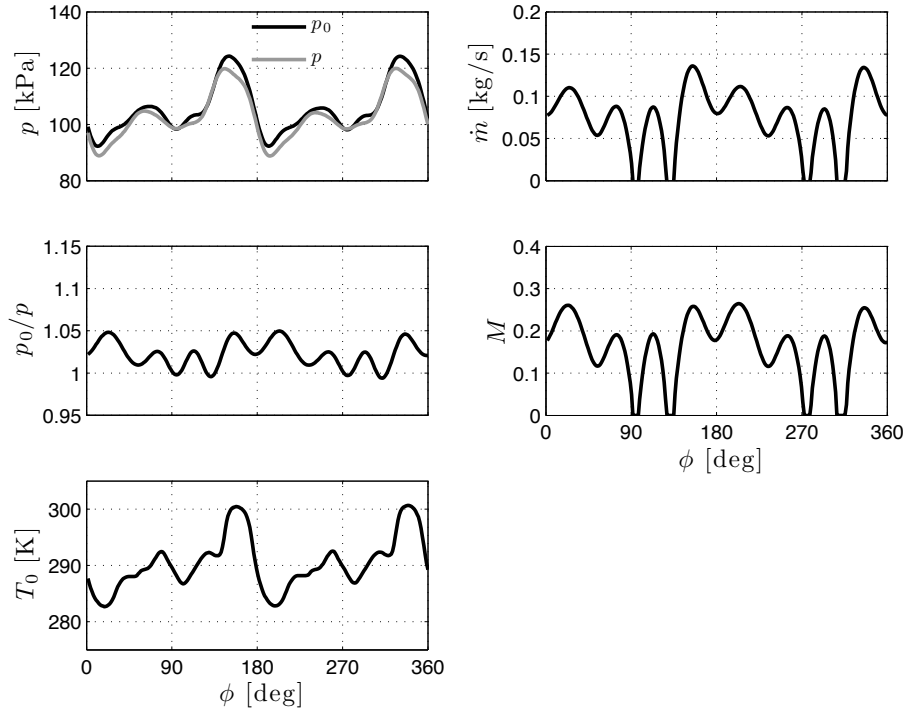
FIGURE 5.13. Pitot tube measured phase averaged quantities
at 80 g/s flow rate and 80 Hz pulse frequency.

and during that period the Mach number and mass flow are set equal to zero.
By averaging the mass flow rate one obtains a flow rate which overestimates the
reference value of 80 g/s by 7.7%. Another possibility would be to average the
pressures and then determine the flow rate from the averaged pressure ratio.
This however give a much larger error, namely an overestimation of the flow
rate with 35%.

For the 80 Hz pulsation case the flow situation becomes more complicated.
Also here one main pressure peak is seen for each pulse from the pulse generator,
however a second smaller peak is also observed. When the pressure ratio is
evaluated a number of peaks are seen but the ratio has much less variation
than in the previous case. Also here there are short instances when the pressure
ratio is below one. Averaging the mass flow rate here gives in contrast to the
40 Hz case, an underestimation of the flow rate by 8.3%. The reason for the
multiple peaks in the pressure is probably due to reflections in the pipe system,
however this needs to be further investigated.

Similar results were obtained for 130 g/s. The deviations from the reference flow rate was at 40 Hz a 1.8% underestimation and at 80 Hz the flow rate was underestimated by less than one percent. The corresponding deviations for the mass flow estimation based on the averaged pressures, are overestimations of 18 and 2.0%, respectively.

5.4. Hot-film flow meter

The two hot films tested were first calibrated under steady flow conditions and thereafter tested under pulsating flow conditions. Typical steady flow calibrations of the two hot film systems are shown in Sec. 4.4.3. Both show an acceptable adherence to the King's law but in this case they are directly calibrated against the mass flow rate such that

$$E^2 = A + B\dot{m}^n \tag{5.7}$$

where A, B and n are all fitted to get the best agreement with the calibration points. For the Scania meter A is very close to E_0^2, i.e. the voltage at zero mass flow rate, but the exponent n is 0.67 which is substantially higher than the original value in Kings law. However one should remember that Kings law is valid for an infinitely long cylinder and the geometry of the hot film sensor is different.

5.4.1. *Pulsating flow*

For the pulsating flow we only show the results for the hot-film sensor provided by Scania. The one manufactured by Bosch did not perform well at any pulse frequencies as is shown in Sec. 5.7.

Here we present results for the case with a mean flow rate of 80 g/s and pulse frequencies, ranging from 4 Hz to 80 Hz. Similar results were also obtained for 130 g/s but these are not presented here. The results for 80 g/s are presented in Fig. 5.14 where the mean mass flow rate as well as the fluctuations around the mean in terms of the *probability density function* (pdf) are presented as function of the pulse frequency. For low pulse frequencies a large span of values are seen in the pdf, indicating that the hot-film is able to resolve the pulsations in the flow. The average value is also close to that measured by the system flow meter, i.e. 80 g/s. The span of the fluctuations gradually decreases up to 20 g/s even though the average value is still consistent with that of the system flow meter. However in the range of 30-50 Hz the hot-film overestimates the flow rate considerably, whereas at higher frequencies ($\geq$ 60 Hz) it becomes again close to the actual value. Another observation is that the span of the mass flow rate fluctuations decreases as the pulse frequency increases, which may be expected since the frequency response of the hot-film system is low.

The over-prediction of the flow rate for medium range pulse frequencies was at first unexplained but was found to be an effect of back flow at the sensor. To
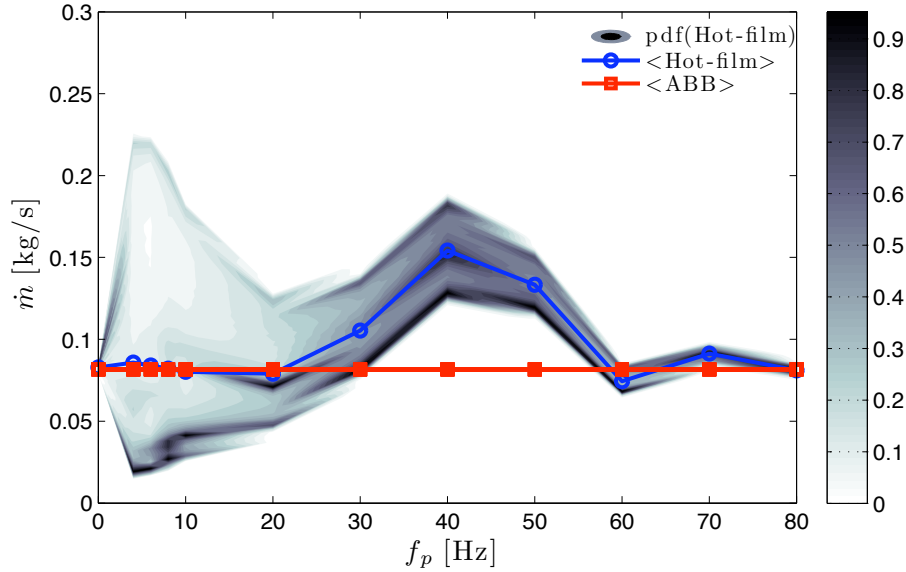
FIGURE 5.14. Mass flow rate measurements with the hot-film flow meter. The estimated mass flow plotted against pulse frequency together with the pdf showing the pulsation range.

investigate this phenomenon, LDV measurements were carried out both inside the pipe and at the pipe outlet, both at the pipe centerline, as mentioned in the previous chapter. For these measurements the PVC pipe was replaced with a Plexiglas pipe without the hot-film sensor in the pipeline. The result from the measurements at the pipe outlet can be seen in Fig. 5.15. Here we can observe substantial amount of back flow at 40 and 50 Hz and smaller amount both at lower and higher pulse frequencies. On the other hand the velocity always seems to be positive at 10, 70 and 80 Hz pulse frequency.

Since the flow pulsations within the pipe may change with the position, due to reflections at the end of the pipe, it was deemed necessary to also measure at the position of the hot-film sensor. These measurements are shown in Fig. 5.16, where the measurements inside and at the pipe outlet are compared for four pulse frequencies, i.e. the right column in Fig. 5.15 is reutilized. It is evident that large back flow occurs for those frequencies that give rise to the largest deviation in mass flow estimation, for the hot-film measurements. At the two lowest frequencies, i.e. 20 and 40 Hz there are a strong correspondence between the measurements at the outlet and inside the pipe, whereas for the higher frequencies the signals seems to be partly out of phase.
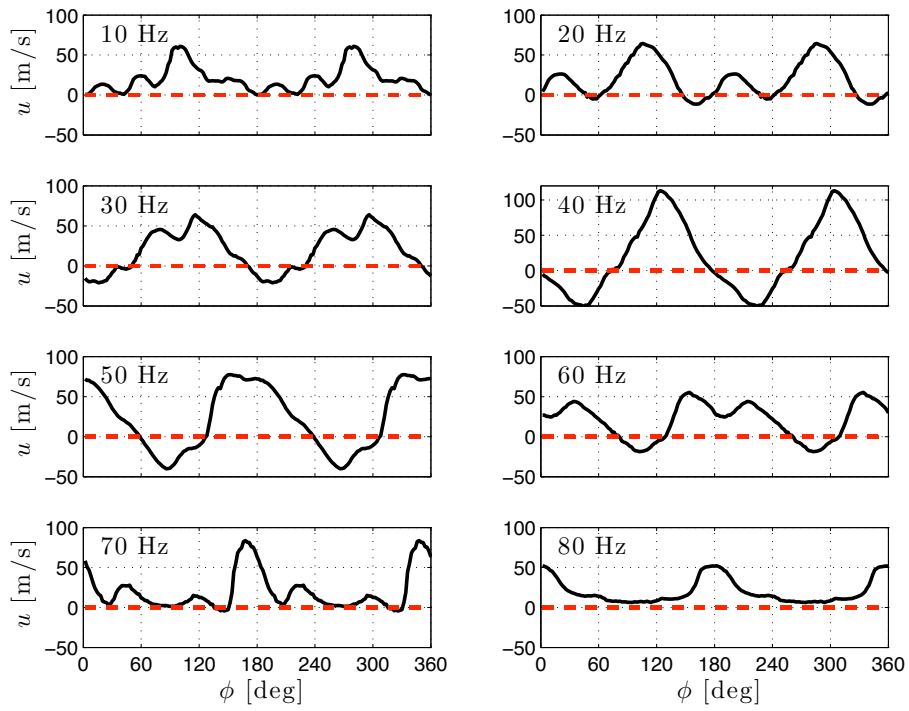
FIGURE 5.15. The phase averaged velocity, measured by LDV at the pipe outlet. The horizontal dashed line is for visual aid.
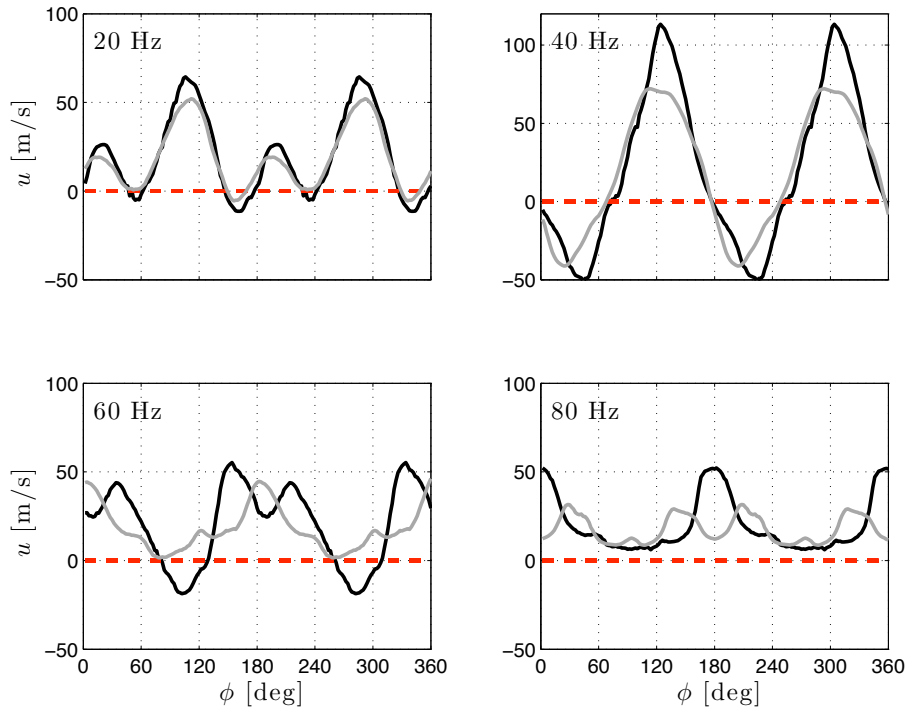
FIGURE 5.16. The phase averaged velocity, measured by LDV. Grey line is measured at the glass section, black line at the outlet.

5.5. Vortex flowmeter

The results from the flowmeter measurements performed with the commercial vortex flowmeter, described in Sec. 4.4.4, are presented here. The sensor of this flowmeter responds to the velocity and the vortex flow meter is therefore in principle sensitive to the volume flow. As shown below this is confirmed by our measurements. The output voltage signal from the vortex flowmeter is averaged in the microprocessor of the vortex meter and therefore the output does not show any variations in time for the pulse frequencies used here. It should be emphasized that the reference mean volume flow determination during both the steady and the pulsating flow measurement is based on the mass flow registered with the ABB system flow meter and an estimation of the average density as described in Sec. 4.4.4.

5.5.1. *Stationary flow*

For the stationary measurements, the vortex flow meter was run at 10 different mass flow rates from 0 g/s up to about 215 g/s, however for the three lowest flow rates the flow meter does not register any flow. Two tests were performed, one with the outlet open to the laboratory and the other with a regulator valve at the outlet. By means of the regulator valve, the pressure in the measuring section could be increased and thereby also the density. This gives a possibility that for a given mass flow rate, the volume flow rate could be changed. Measurements were made at the same mass flow rates for the two cases and these results can be seen in Fig. 5.17, where the output signal E_{out}, is plotted versus the volume flow rate Q. As can be seen there is a linear relationship between the volume flow rate and the output of the vortex flow meter. One can notice from the plot that the squares (representing non-pressurized flow), is shifted upwards to a higher volume flow rate compared to the circles (representing pressurized flow). This is (somewhat trivially) due to the fact that the volume flow rate will increase if the density is lowered, for a given mass flow rate.
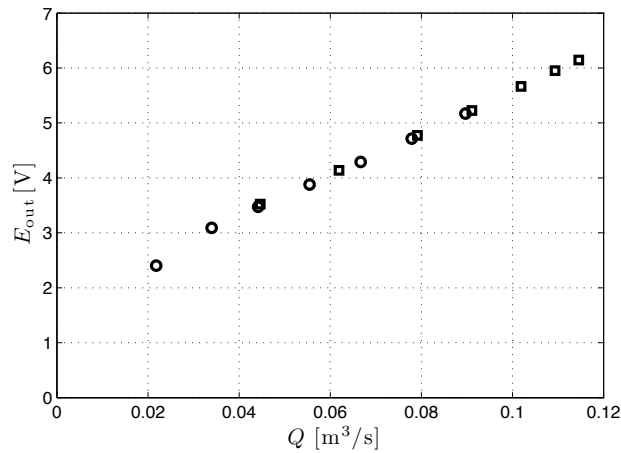
FIGURE 5.17. The vortex flow meter output as function of the volume flow rate. ○: Pressurized flow, □: Non-pressurized flow.

5.5.2. *Pulsating flow*

For pulsating flows the averaging process of the vortex flow meter gives fairly accurate results for all pulse frequencies as shown in Sec. 5.7, also in the pulse frequencies where we would expect back-flow. Note that the instantaneous density is estimated with pressure measurements upstream and downstream

the vortex flowmeter, together with measurements of the stagnation pressure and temperature downstream the flowmeter.

5.6. Turbine flow meter

The turbine flow meter measurements were done both in stationary and pulsating flow. Similarly to the vortex flow meter the turbine flow meter senses the volume flow as will be shown below and therefore the density needs to be determined. This is done by measuring the pressure and stagnation temperature in a similar way as was done with the vortex flow meter.

5.6.1. *Stationary flow*

Also for the turbine flow meter two test were made for the stationary flow case, one with the outflow direct to the laboratory and the other with a regulating valve at the outflow in order to verify that the flow meter responds to the volume flow. 10 mass flow rates were used, starting at 0 g/s going up to about 215 g/s. For the non-pressurized case the pressure downstream the flow meter varies between 0 and 50 kPa above ambient, whereas for the pressurized case it is kept at 100 kPa above ambient.

The corresponding measurements for the turbine flow meter under pressurized and non-pressurized conditions are given in Fig. 5.18. The output is fairly linear with the flow rate, and as can be seen the pressurized and non-pressurized measurement points seem to collapse on the same line, hence showing that turbine flow meter responds to volume flow rate and that the output is independent of the density.
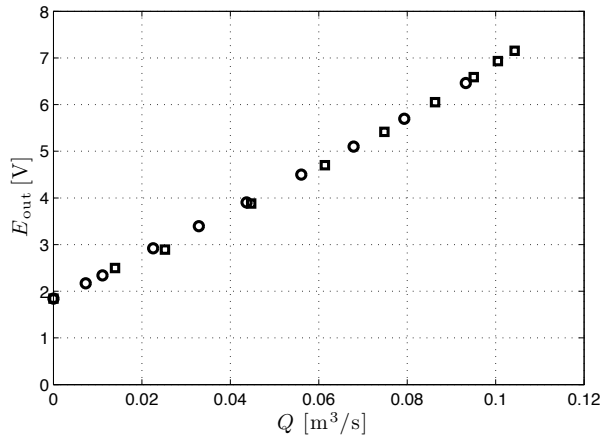

FIGURE 5.18. The turbine flow meter output as function of the volume flow rate. ○: Pressurized flow. □ Non-pressurized flow.

The output from the turbine flow meter did not show the pulsations but was steady. The pulsating flow results are be presented in Sec 5.7. For the low frequencies the turbine flow meter show too high values, but for the higher frequencies one obtains values that are within $\pm1\%$ of the value obtained from the system mass flow meter. One should note that these values are obtained, using the average density over the pulse, from the pressure measurements on both sides of the turbine flow meter as well as the stagnation temperature.

5.7. Summary

This section summarizes the behavior of the flowmeters in pulsating flow in Table 4. The HWMFM was only studied for two pulse frequencies (40 Hz and 60 Hz respectively). Furthermore, it should be emphasized that these values depends on how the averaging procedure is done. Common for all values presented here, is that they are based on the time resolved mass flow rate. Finally, for the flow meters where pressure measurements are used to estimate the mass flow rate, the values do also depend on how the filtering of the pressure signals are done, albeit to a small degree.

TABLE 4. Mean mass flow rate for different flow meters at pulsating conditions and at the reference rate ~ 80 g/s[1] . The flow rates are normalized with the reference flow meter. Hot-film 1 is from Bosch and Hot-film 2 is from Scania.

Flowmeter	10 Hz	20 Hz	30 Hz	40 Hz	50 Hz	60 Hz	70 Hz	80 Hz
HWMFM	-	-	-	1.00	-	1.01	-	-
Venturi	1.02	1.06	1.09	1.05	1.00	1.01	1.00	1.02
Pitot	0.95	1.04	1.18	1.07	0.95	0.92	0.95	0.92
Hot-film 1	0.64	0.92	1.00	1.57	1.25	0.60	0.66	0.47
Hot-film 2	0.98	0.97	1.29	1.89	1.63	0.92	1.12	1.00
Vortex	0.98	0.99	1.08	1.01	0.97	1.00	0.97	1.00
Turbine	1.24	1.21	1.18	1.07	1.03	1.00	1.01	1.00

[1] The deviation from this value is for all cases less than 3%.

Vortex shedding flow meter using wavelet analysis

In addition to the commercial flow meters described in Chap. 5 a new set-up based on the vortex shedding principle was developed. It was realized that such a vortex shedder can be used to actually resolve pulsations if the vortex shedding frequency is substantially higher than the pulsating frequency. By using wavelet analysis it was found that the instantaneous flow rate could be determined as described in detail in Laurantzon *et al.* (2010*b*), Paper 3. For further information of the set-up the reader is referred to that paper. In this chapter some more features of the device are demonstrated.

6.1. Stationary flow

The experiment for the stationary case was carried out for five flow rates. The vortex shedding behind a cylinder with a diameter of 3 mm was detected by means of a 5 μm hot-wire probe. The time signal was then analyzed using power spectrum for each flow rate. A clear peak in the energy spectrum for each flow rate was obtained. In Fig. 6.1, the vortex shedding frequency f_{vs} is plotted versus the bulk velocity u_b and a near linear dependence between the shedding frequency and the bulk flow can be observed. The Reynolds number for the lowest velocity (10 m/s) is about 2000 which is high enough for the Strouhal number St= fd/u to be constant.

In Fig. 6.2 the vortex shedding frequency is plotted versus the frequency estimated from the bulk velocity, f_b. Here f_b is obtained as Stu/d where the Strouhal number is given the generally accepted value for a circular cylinder, namely St= 0.21[1]. As can be seen there is a good agreement between the estimated and measured frequency.

6.2. Pulsating flow

The idea behind using the vortex shedding cylinder for pulsating flows is that it should be able respond to changes in the pulsating frequency as long as the pulsating frequency is much lower than the shedding frequency, and that the relation between the shedding frequency and the bulk flow should adhere to

---

[1]This value is confirmed from many laboratory experiments, see for example Kundu & Cohen (2004).
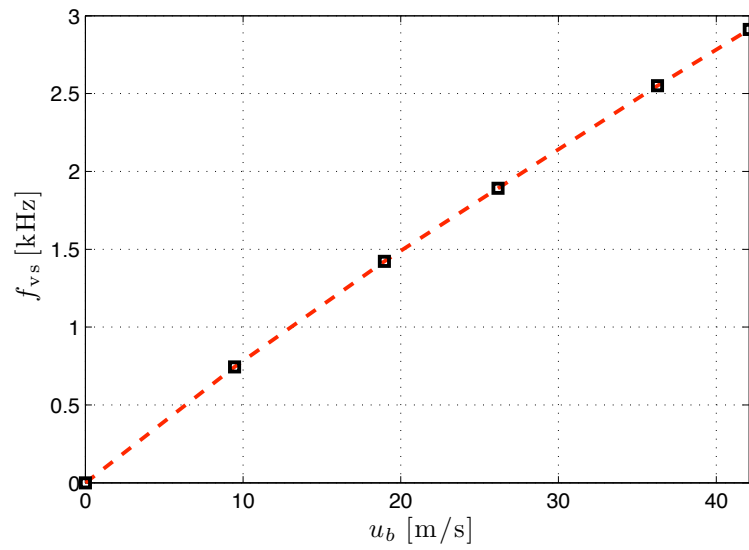
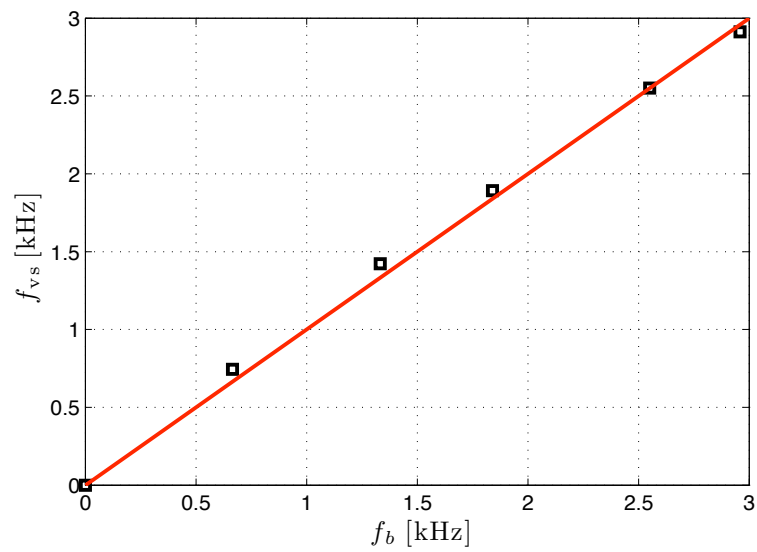FIGURE 6.1. The vortex shedding frequency vs. the bulk velocity. The cylinder diameter was 3 mm.

FIGURE 6.2. The shedding frequency vs. the estimated frequency obtained from the bulk velocity. Based on the same data as in Fig. 6.1

the calibration shown in Fig. 6.1. This has been tested with good results in Laurantzon *et al.* (2010*b*), Paper 3. However in that case all measurements were conducted without back flow. This was accomplished by means of mixing the pulsating flow with a constant flow through a bypass branch parallel to the pulse generator. Here additional measurement are presented, where the bypass branch was closed, which gives rise to back flow for certain pulse frequencies and flow rates as was also observed for the measurements presented in Chap. 5. With this exception, there were no further changes in the set-up as compared to Laurantzon *et al.* (2010*b*)

In Fig. 6.3, the velocity obtained from the vortex shedding measurements and the subsequent wavelet analysis, is compared with hot-wire and LDV measurements. As can be seen from the LDV measurements, there is a period of back flow during the pulse cycle. During this period the hot-wire sensor registers the absolute value of the velocity, which becomes almost a perfect mirror image of the "true" velocity as obtained from the LDV measurement. The vortex shedding flowmeter does not yield a signal when back flow prevails, but for the rest of the pulse period there is an excellent agreement between the three methods, despite the fact that the hot-wire and LDV measurements are at one point in space. This is probably due to the fact that during pulsating conditions the flow has the before described top-hat profile.
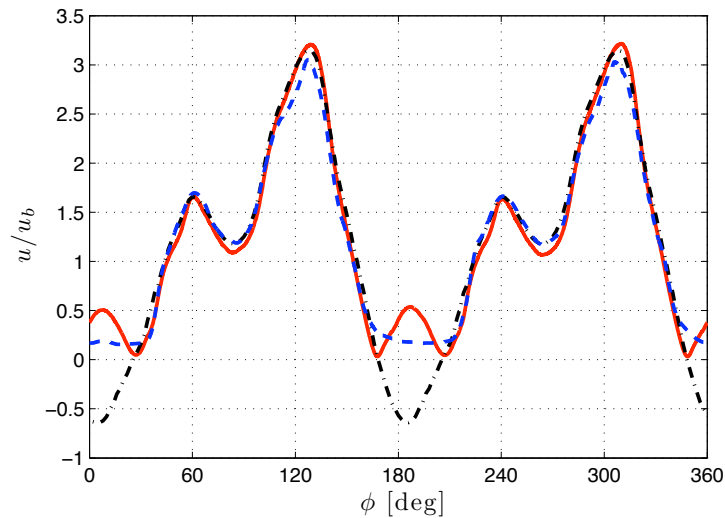

FIGURE 6.3. The velocity scaled with the bulk velocity u_b, obtained from vortex shedding (dashed), hot-wire (solid) and LDV measurement (dashed-dot). Here, $f_p = 40$ Hz and $\dot{m} = 25$ g/s

In addition to the flow case in Fig. 6.3, measurement of some different pulse frequencies were performed. The result for this is presented in Table 1. The mass flow rate obtained with the vortex flow meter is based on the velocity (from the wavelet analysis), the atmospheric density ($\rho = 1.20\ kg/s$), and the cross section area of the pipe. The case from Fig. 6.3 is shown in the table, and as can be seen, at that frequency the flow rate is overestimated with 13%. This overestimation is expected, because evidently there is back flow at this pulsating frequency.

Flow rate	0 Hz	20 Hz	40 Hz	60 Hz
25 g/s	1.06	1.01	1.13	0.941

TABLE 1. Mass flow rate obtained with the vortex shedding flow meter, normalized with the reference flow rate.

In order to verify the assumption that the vortex flow meter registers a velocity close to the bulk flow rate, regardless of the radial position of the hot-wire probe, two measurement series were performed. The first measurement series was conducted with the hot-wire probe located in the wake downstream the cylinder and was traversed in the axial direction of the cylinder. The first measurement point was about 2 mm from the pipe wall and measurements were made in steps of 2 mm from this point to the centerline of the pipe. For the second measurement series, the previous measurements were repeated under the same flow conditions, but with the cylinder removed. Thus providing means to measure the velocity directly with the (calibrated) hot-wire. The comparison between the velocity measurements obtained with the vortex flow meter and the velocity measurements with the hot-wire is shown in Fig. 6.4, where one can see that the velocity determined with the vortex flow meter is virtually the same for each measurement point, whereas for the hot-wire measurements, the lower velocity close to the pipe wall is apparent.
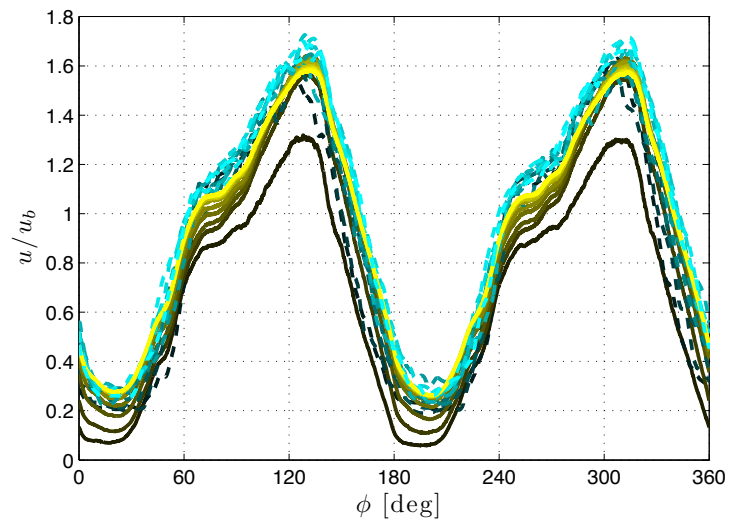
FIGURE 6.4. The phase averaged velocity obtained with HWA (solid lines) and vortex flow meter (dashed lines), scaled with the bulk velocity u_b. The brighter the color, the closer the centerline.

CHAPTER 7

Concluding remarks

This thesis reports on a number of flow meters that are more or less suitable to measure mass flow rates in compressible flows under steady and pulsating conditions. Some of the flow meters are shown to measure volume flow and it hence necessary to determine the density in order to obtain the mass flow rate. It is shown that in systems with pulsating compressible flow, back flow may occur and can severely corrupt the measured mean mass flow rate.

Based on the results from Chap. 5, a short summary and discussion will follow for each flow meter evaluated. It should be emphasized that the flow situation may not be the same at the measuring section of the flow meters, even if the flow rate and pulsating frequency are the same. Depending on the pipe dimensions as well as their connection upstream and downstream the flow meter in question, the transmitted and reflected pressure waves can interact in quite different ways. For instance, as one could notice, for certain pulsating frequencies back flow was predominate during a longer period of the pulse, whereas it did not occur for other flow condition (for the one and same flow meter set-up).

7.1. HWMFM

- For this kind of flow meter one can not be fully aware of when back flow occurs. Studying the time signal can give a hint if back flow occurs; if the velocity tends to zero and then slightly increases to go back to zero again, then it is likely that there is back flow. This would be as we have seen in Chap. 5 a mirror image of what the LDV measurements gives at back flow.
- Since the estimation of flow rate is fair for all cases studied, the back flow, if any, is small which also can be deduced from the time signals. However, to obtain better results the temperature should be simultaneously measured.

7.2. Venturi

- During pulsating conditions it was found to important to resolve the instantaneous pressure to be able to calculate the instantaneous mass flow rate which then can be averaged to obtain the mean flow rate.

This is especially important if the flow is choked during part of the pulse cycle.

- The venturi shows good agreement with the actual flow rate for most pulsating frequencies. The highest deviation is 9%, which can be due to back flow.
- As any other flow meters where the flow rate is based on pressure measurements, the accuracy will be poor at low flow speeds. This can give an error if the velocity is low during a large portion of the pulsations.

7.3. Pitot tube

- The Pitot tube measurements do not give as good estimation of the flow rate as the venturi. One should recall that the Pitot tube gives more or less "a point in space" measurement, in contrast to most of the other flow meters. The assumption made was that the flow profile was the same in both steady and pulsating flow. From the HWMFM measurements it is known that the velocity profile during pulsations has a top-hat character which would then give an underestimation of the mass flow rate if it is calibrated against the stationary profile.

7.4. Hot-film

- As could be seen in Chap. 5, the inability to sense back flow can give rise to a large overestimation of the flow rate.
- For pulse frequencies when back flow is not occurring, the Scania flow meter output agrees well with the actual flow rate.
- When the Bosch flow meter is used in the present set-up it did not give acceptable results during any of the pulse cycle conditions tested.

7.5. Vortex flow meter

- This device handle the pulsating flow quite well; The largest deviation from the actual flow rate is 8% at 30 Hz. However, this seems to be a flow condition where back flow occurs for most of the meters since they all overestimate the flow rate.

7.6. Turbine flow meter

- The turbine flow meter overestimates the flow rate rather much for the three lowest pulsation frequencies, but shows good agreement for higher frequencies. The overestimation for turbine flow meters in pulsating flow, is well known, as discussed in Chap. 3.

7.7. In-house vortex shedder using wavelet analysis

In addition to the results from the more or less commercial flow meters described above an in-house flow meter set-up based on the vortex shedding from

a cylinder was tested using a new signal analyzing technique (see Chap. 6). By using the wavelet technique it was possible to obtain a time-resolved flow rate from the vortex shedding signal also under pulsating conditions. Although this method has so far only been tested for rather low flow rates it bears the potential also for measurements at higher flow rates. The critical point is the time response of the detecting hot wire, but by increasing the diameter of the shedding wire the frequency decreases. For instance for a wire with 3 mm diameter the shedding frequency is about 10 kHz at 150 m/s which should be possible to accurately detect with a suitable hot-wire anemometer.

Future plans includes investigating the potential of this set-up to accurately determine the average flow rate in various set-ups, under pulsating conditions and for non-ideal inflow conditions, such as skewed profiles or flow rotation. For engine gas exchange applications this method could be valuable to use to measure the time dependent flow rate before and after the turbine of a turbocharger as well as before and after an EGR-cooler to investigate how flow pulsations are damped. It may also be used to e.g. measure the time dependent flow rate into an engine cylinder during the intake valve opening cycle or the pulsating exhaust flow from a cylinder (of course only during simulated cold conditions).

CHAPTER 8

Papers and authors contributions

Paper 1
The corona mass flow meter
F. Laurantzon (FL), N. Tillmark (NT) & P. H. Alfredsson (HAL).
The 19th Symposium on Measuring Techniques in Transonic and Supersonic Flow in Cascades and Turbomachines

This work is of experimental character. The experimental set-up was designed by FL and NT. The experiments was carried out by FL under supervision of HAL and NT. The writing was done jointly, by FL, HAL and NT. The work has been presented at the von Karman Institute, Belgium, 2008.

Paper 2
A pulsating flow rig for analyzing turbocharger performance
F. Laurantzon (FL), N. Tillmark (NT) & P. H. Alfredsson (HAL).
9th International Conference on Turbochargers and Turbocharging

This work presents a flow rig for turbocharger related research. The experimental set-up was designed by NT. The experiments were performed by FL, under supervision of HAL and NT. The writing was done jointly, by FL, HAL and NT. The work has been presented at Institution of Mechanical Engineers, London, 2010.

Paper 3
Time-resolved measurements with a vortex flowmeter in a pulsating turbulent flow using wavelet analysis
F. Laurantzon (FL), R. Örlu (RÖ), A. Segalini (AS) & P. H. Alfredsson (HAL).
Meas. Sci. Tech. **21** (2010)

This work introduces a novel method, based on wavelet analysis to extract time resolved velocity from the signal of a vortex shedder. The experimental set-up was designed by HAL and FL. The experiments were performed by FL, under supervision of HAL. The wavelet analysis code was provided by AS. The paper was written by RÖ with contributions from FL and input from AS and HAL. The work was published in Measurement Science and Technology.

Paper 4
Review on the sensed temperature in cold-wire and hot-wire anemometry
F. Laurantzon (FL), A. Kalpakli (AK), R. Örlu (RÖ), & P. H. Alfredsson (HAL).
Technical CICERO report

This work is a review on the measured temperature by means of cold-wires and is supplemented by experiments. The experiments were performed by AK and RÖ. The data analysis was done by FL. The report was written by AK and RÖ with input from FL and HAL. The report is a work in progress and is planed to be submitted.

Acknowledgements

APPENDIX A

Venturi flowmeter plots

In this section, four complementary plots to the ones from Sec. 5.2.2 are shown.
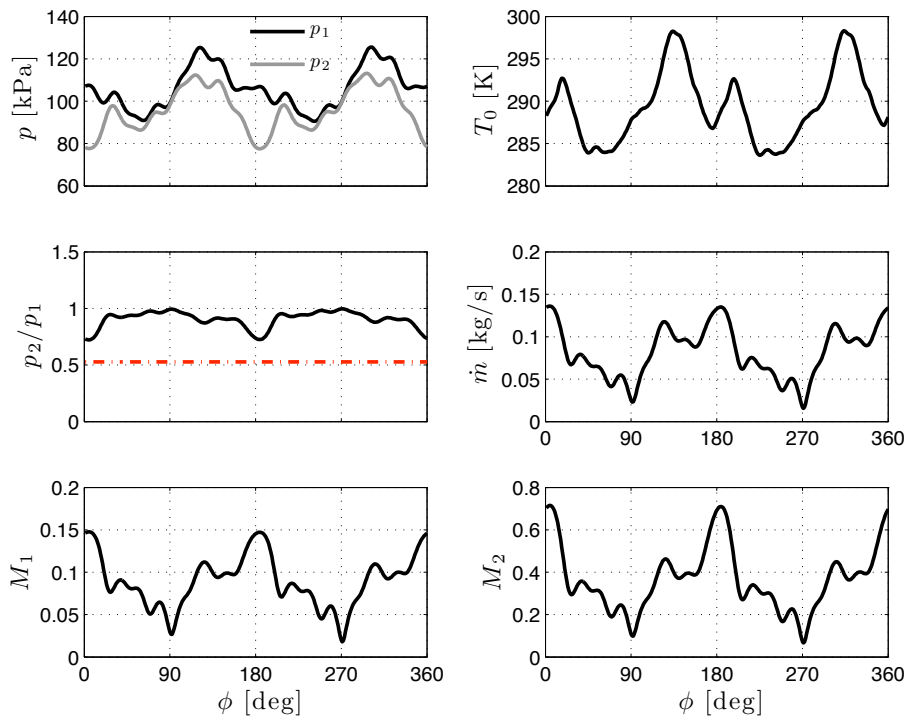

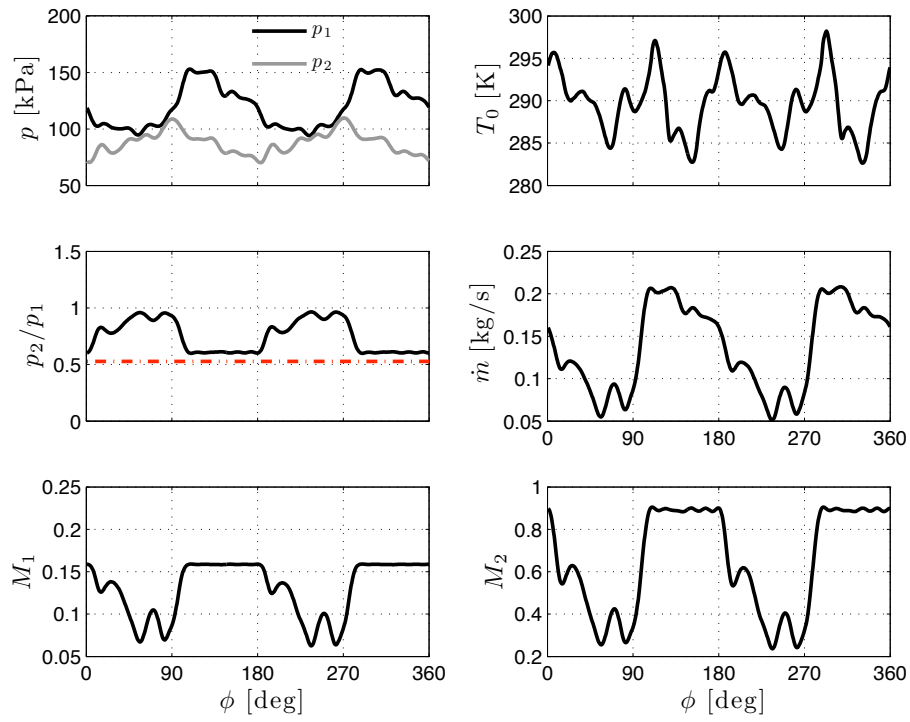FIGURE A.1. Phase averaged data at 80 g/s and 60 Hz pulsating frequency.

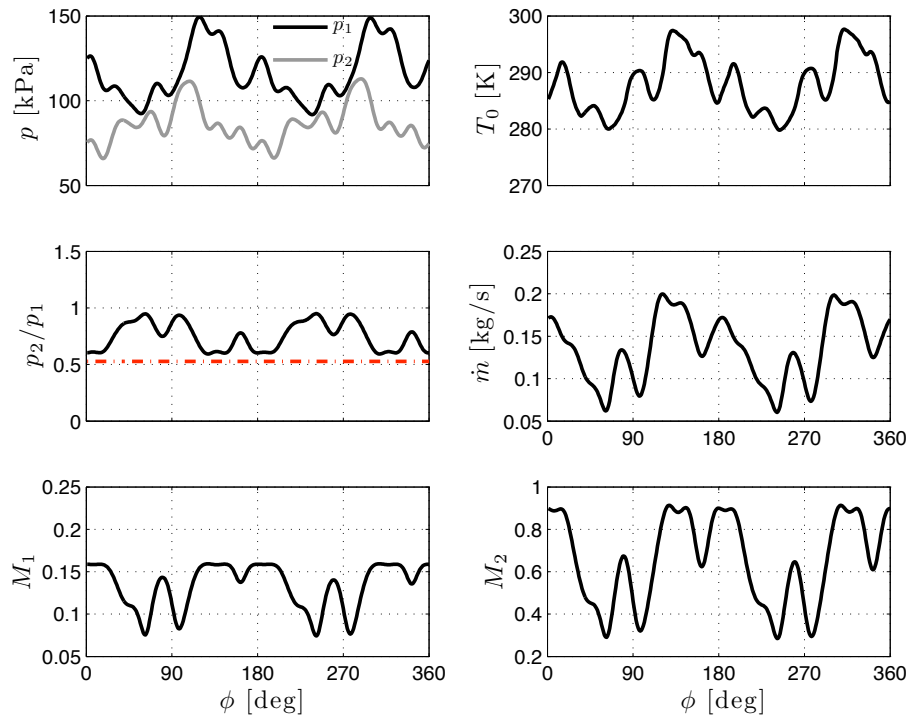FIGURE A.2. Phase averaged data at 130 g/s and 40 Hz pulsating frequency.

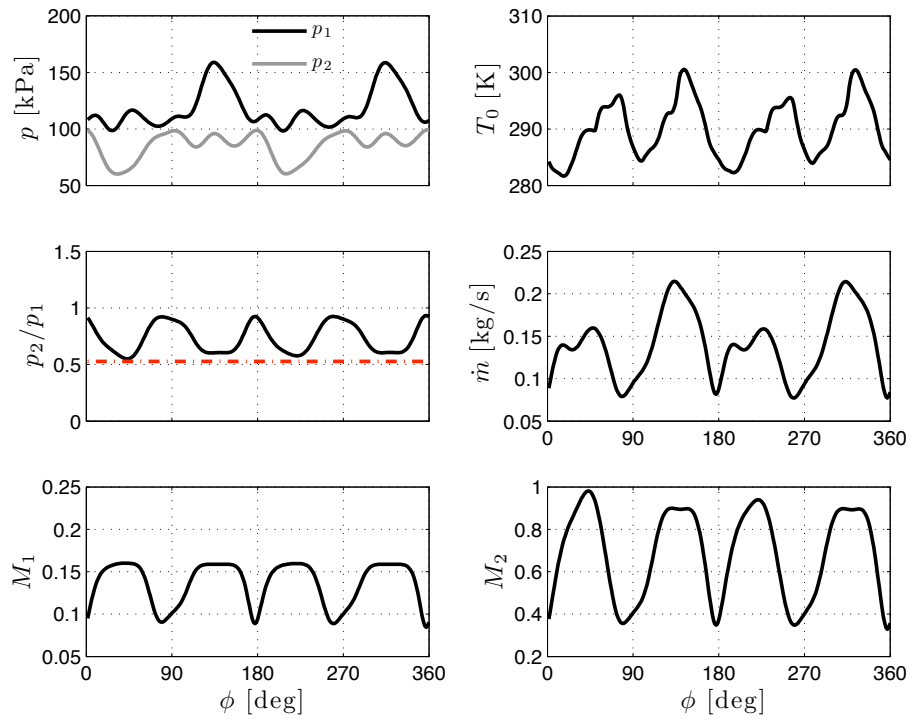FIGURE A.3. Phase averaged data at 130 g/s and 60 Hz pulsating frequency.

FIGURE A.4. Phase averaged data at 130 g/s and 80 Hz pulsating frequency.

References

ANDERSON, J. 2003 *Modern Compressible Flow: With Historical Perspective*, 3rd edn. McGraw-Hill.

BAKER, R. C. 2000 *Flow measurement handbook*. Cambridge University Press, Cambridge, UK.

BRUUN, H. H. 1995 *Hot-wire anemometry: principles and signal analysis*. Oxford University Press Inc., New York, USA.

CASCETTA, F. 1995 Short history of the flowmetering. *Isa Transactions* **34**, 229–243.

CHEESEWRIGHT, R. & CLARK, C. 1998 The effect of flow pulsations on coriolis mass flow meters. *J. Fluid Struct.* **12**, 1025–1039.

CHEN, J. & DAVIDSON, J. H. 2002 Electron density and energy distributions in the positive dc corona: interpretation for corona-enhanced chemical reactions. *Plasma Chem. Plasma. P.* **22**, 199–224.

GAJAN, P., MOTTRAM, R. C., HEBRARD, P., ANDRIAMIHAFY, H. & PLATET, B. 1992 The influence of pulsating flows on orifice plate flowmeters. *Flow Meas. Instrum.* **3**, 118–129.

HÅKANSSON, E. & DELSING, J. 1994 Effects of pulsating flow on an ultrasonic gas flowmeter. *Flow Meas. Instrum.* **5**, 93–101.

HEBRARD, P., MALARD, L. & STRZELECKI, A. 1992 Experimental study of a vortex flowmeter in pulsatile flow conditions. *Flow Meas. Instrum.* **3**, 173–186.

ISO-5167 2003 *Measurement of fluid flow by means of pressure differential devices inserted in circular cross-section conduits running full*.

KING, L. V. 1914 On the convection of heat from small cylinders in a stream of fluid: determination of the convection constants of small platinum wires with applications to hot-wire anemometry. *Phil. Trans. R. Soc. A* **214A**, 373–432.

KUNDU, P. K. & COHEN, I. M. 2004 *Fluid Mechanics*, 3rd edn. Elsevier Academic Press.

LAURANTZON, F., KALPAKLI, A., ÖRLÜ, R. & ALFREDSSON, P. H. 2010*a* Review on the sensed temperature in cold-wire and hot-wire anemometry. *Technical CICERO report* .

LAURANTZON, F., ÖRLÜ, R., SEGALINI, A. & ALFREDSSON, P. H. 2010*b* Time-resolved measurements with a vortex flowmeter in a pulsating turbulent flow using wavelet analysis. *Meas. Sci. Technol.* **21**.

Laurantzon, F., Tillmark, N. & Alfredsson, P. H. 2008 The corona mass flow meter. In *The 19th Symposium on Measuring Techniques in Transonic and Supersonic Flow in Cascades and Turbomachines*.

Laurantzon, F., Tillmark, N. & Alfredsson, P. H. 2010c A pulsating flow rig for analyzing turbocharger performance. In *9th International Conference on Turbochargers and Turbocharging*.

Massey, B. & Ward-Smith, J. 1998 *Mechanics of fluids*, 7th edn. Nelson Thornes.

McKee, R. J. 1992 Pulsation effects on single-and two-rotor turbine meters. *Flow Meas. Instrum.* **3**, 151–166.

Merzkirch, W. 2005 *Fluid mechanics of flow metering*. Springer-Verlag, Berlin Heidelberg.

Mottram, R. C. 1992 Introduction: An overview of pulsating flow measurement. *Flow Meas. Instrum.* **3**, 114–117.

Nakamura, H., Asano, I., Adachi, M. & Senda, J. 2005 Analysis of pulsating flow measurement of engine exhaust by a pitot tube flowmeter. *Int. J. Engine Res.* **6**, 85–93.

Omega 1995 *Complete Flow and Level Measurement Handbook and Encyclopedia*. OMEGA Press.

Örlü, R. 2006 Experimental study of passive scalar mixing in swirling jet flows. Teknl thesis, KTH Mechanics, Royal Institute of Technology.

Sanderson, M. 1989 Editorial. *Flow Meas. Instrum.* **1**, 3 – 4.

Sieverding, C. H., Arts, T., Denos, R. & Brouckaert, J. F. 2000 Measurement techniques for unsteady flows in turbomachines. *Exp. Fluids* **28**, 285–321.

Tavoularis, S. 2005 *Measurement in fluid mechanics*. Cambridge University Press.

Van Dijk, A. 1999 Aliasing in one-point turbulence measurements: theory, DNS and hotwire experiments. PhD thesis, Delft University of Technology.

Vetter, G. & Notzon, S. 1994 Effect of pulsating flow on coriolis mass flowmeters. *Flow Meas. Instrum.* **5**, 263 – 273.